Functional identification of the input–output transforms of motoneurones in the rat and cat

Andrew V. Poliakov, Randall K. Powers and Marc D. Binder *

Department of Physiology & Biophysics, School of Medicine, University of Washington, Seattle, WA 98195, USA

1. We studied the responses of rat hypoglossal and cat lumbar motoneurones to a variety of excitatory and inhibitory injected current transients during repetitive discharge. The amplitudes and time courses of the transients were comparable to those of the synaptic currents underlying unitary and small compound postsynaptic potentials (PSPs) recorded in these cells. Poisson trains of ten of these excitatory and ten inhibitory current transients were combined with an additional independent, high-frequency random waveform to approximate band limited white noise. The white noise waveform was then superimposed on long duration (39 s) suprathreshold current steps.

2. We measured the effects of each of the current transients on motoneurone discharge by compiling peristimulus time histograms (PSTHs) between the times of occurrence of individual current transients and motoneurone discharges. We estimated the changes in membrane potential associated with each current transient by approximating the passive response of the motoneurone with a simple resistance–capacitance circuit. The relations between the features of these simulated PSPs and those of the PSTHs were similar to those reported previously for real PSPs: the short-latency PSTH peak (or trough) was generally longer than the initial phase of the PSP derivative, but shorter than the time course of the PSP itself. Linear models of the PSP to PSTH transform based on the PSP time course, the time derivative of the PSP, or a linear combination of the two parameters could not reproduce the full range of PSTH profiles observed.

3. We also used the responses of the motoneurones to the white noise stimulus to derive zero-, first- and second-order Wiener kernels, which provide a quantitative description of the relation between injected current and discharge probability. The convolution integral computed for an injected current waveform and the first-order Wiener kernel should provide the best linear prediction of the associated PSTH. This linear model provided good matches to the PSTHs associated with a wide range of current transients. However, for the largest amplitude current transients, a significant improvement in the PSTH match was often achieved by expanding the model to include the convolution of the second-order Wiener kernel with the input.

4. The overall transformation of current inputs into firing rate could be approximated by a second-order Wiener model, i.e. a cascade of a dynamic, linear filter followed by a static non-linearity. At a given mean firing rate, the non-linear component of the response of the motoneurone could be described by the square of the linear component multiplied by a constant coefficient. The amplitude of the response of the linear component increased with the average firing rate, whereas the value of the multiplicative coefficient in the non-linear component decreased. As a result, the overall transform could be predicted from the mean firing rate and the linear impulse response, yielding a relatively simple, general description of the motoneurone input–output function.

* To whom correspondence should be addressed.

The activation of one or more presynaptic neurones is associated with a transient change in the discharge probability of a tonically discharging postsynaptic cell. The change in firing probability can be measured by compiling a cross-correlation or peristimulus time histogram (PSTH) between the spikes of the postsynaptic (response) neurone and those of the presynaptic (stimulus) neurones (Moore, Perkel & Segundo, 1966). The time course of the initial change in firing probability associated with the arrival of a synaptic input has been called the primary correlation kernel (Knox, 1974), and the quantitative relation between this function and the underlying postsynaptic potential (PSP) has been called the primary correlation (PC) operator (Kirkwood & Sears, 1978). As noted by Kirkwood (1979), knowledge of the PC operator would provide a number of benefits, including the ability to estimate the strength of a synaptic input from the features of the primary correlation kernel. In turn, the effects of activity in a population of presynaptic neurones on the discharge of a postsynaptic cell can theoretically be predicted from measurements of synaptic potentials (Fetz, Cheney, Mewes & Palmer, 1989).

A general quantitative expression for the PC operator has remained elusive, despite over twenty years of research on the topic. Kirkwood & Sears (1978) proposed that in the case of small unitary EPSPs superimposed upon a high level of background noise, the PC operator takes the form of a linear combination of the PSP and its derivative. However, this formulation does not appear to hold in general. For excitatory inputs, the relative contribution of the PSP and its derivative to the primary correlation kernel depends upon the ratio of the EPSP amplitude to that of the background synaptic noise (Fetz & Gustafsson, 1983; Gustafsson & McCrea, 1984; Cope, Fetz & Matsumura, 1987). Moreover, the primary correlation kernels produced by large inhibitory inputs (IPSPs) do not resemble a linear combination of the IPSP and its derivative (Fetz & Gustafsson, 1983). In addition, there are secondary features in the cross-correlation histogram arising from periodicities in the discharge of the pre- and postsynaptic neurones that complicate the interpretation of histogram features (Moore, Segundo, Perkel & Levitan, 1970). Further, non-linear interactions between pre- and postsynaptic neurones have been revealed in higher-order cross-correlation functions (reviewed in Conway, Halliday & Rosenberg, 1993).

An alternative method of describing synaptically evoked changes in discharge probability is to relate them to the synaptic current rather than to the change in membrane potential produced by that current. This method has the advantage that transient synaptic inputs can be simulated by intracellular current injection under standard current-clamp conditions (Reyes & Fetz, 1993; Powers & Binder, 1996; Poliakov, Powers, Sawczuk & Binder, 1996), allowing precise experimental control of the time course and amplitude of the simulated synaptic input. A transfer function relating the effects of synaptic current on discharge probability can then be derived by testing the effects of a wide array of

injected current waveforms. An efficient method of deriving such a general transform is through the application of the white noise method of system identification (reviewed in Marmarelis & Marmarelis, 1978; Sakai, 1992). This method is particularly appropriate for the analysis of non-linear systems.

The goal of the present experiments was to implement the white noise method to characterize the transformation of injected current waveforms into changes in motoneurone firing rate. Repetitive discharge was elicited in rat hypoglossal motoneurones *in vitro* and cat lumbar motoneurones *in vivo* by injecting a current waveform composed of a suprathreshold current step with superimposed white noise. We designed the white noise stimulus so that it contained trains of specific current transients that mimicked those underlying individual PSPs. We used the responses of the motoneurones to compute the zero-, first- and second-order Wiener kernels. A series of orthogonal functionals derived from these kernels provides an approximation of the input–output function of the motoneurone. The first-order Wiener kernel gives the best-fit linear approximation of the response of the motoneurone to a current impulse. Moreover, a second-order Wiener model (a series of functionals including the zero-, first- and second-order Wiener kernels) accounted for both the average firing rate and most of the non-linearity inherent in the responses of the motoneurone to both depolarizing and hyperpolarizing current transients. Further, we found that the overall transformation of current inputs into firing rate could be approximated by the Wiener model, i.e. a cascade of a dynamic, linear filter followed by a static non-linearity.

We compared the capacity of several different transforms to predict the responses of the motoneurones to the defined depolarizing and hyperpolarizing current transients embedded in the white noise input signal. Of the several linear models tested, we found that the predictions based on the first-order Wiener kernel provided the best match to the PSTHs elicited by a wide range of current transient waveforms. However, this linear transform systematically underestimated the excitatory effects of the largest depolarizing current transients and overestimated the inhibitory effects of the larger hyperpolarizing current transients. The addition of the second-order, non-linear term to the system allowed us to provide a close match to all of the observed PSTHs. Portions of this material have been presented in abstract form (Poliakov, Powers, Sawczuk & Binder, 1995; Poliakov, Powers & Binder, 1996).

METHODS

Experimental preparation

The basic surgical and experimental procedures we used to obtain intracellular recordings from cat lumbar motoneurones *in vivo* and rat hypoglossal motoneurones *in vitro* have been described in detail in recent publications from this laboratory (Sawczuk, Powers & Binder, 1995; Powers & Binder, 1996; Poliakov *et al.* 1996). Only the key features will be briefly described here.

Rat hypoglossal motoneurones were studied in 400 μm thick brainstem slices obtained from 3- to 5-week-old Sprague–Dawley rats. Following the induction of anaesthesia with an intramuscular injection of a mixture of ketamine (68 mg kg^{-1}) and xylazine (4 mg kg^{-1}), a section of brainstem was removed and glued to a Plexiglass tray filled with cooled, artificial cerebrospinal fluid in which Na$^+$ had been replaced with sucrose (S-ACSF; composed of (mm): 220 sucrose, 2 KCl, 1·25 NaH$_2$PO$_4$, 26 NaHCO$_3$, 2 MgCl$_2$, 2 CaCl$_2$ and 10 glucose). A series of transverse slices were cut throughout the length of the hypoglossal nucleus, transferred to a holding chamber and incubated at room temperature (19–21 °C) in S-ACSF for 30 min, followed by 30 min incubation in standard ACSF (the same as S-ACSF except that sucrose was replaced with 126 mm NaCl). For the experimental recordings, the slices were submerged in a recording chamber and perfused with ACSF warmed to a temperature of 26–30 °C. We used glass micropipettes filled with 3 m KCl (electrode resistances of 30–60 MΩ) to obtain intracellular recordings from hypoglossal motoneurones. Moto-neurone identity was based on location and on the similarity of cell properties to those reported by previous investigators (Haddad, Donnelly & Getting, 1990; Viana, Bayliss & Berger, 1995; Sawczuk et al. 1995).

Cat lumbar motoneurones were studied in intact pentobarbitone anaesthetized cats. Anaesthesia was induced with a 40 mg kg^{-1} intraperitoneal injection of pentobarbitone, and supplemental intra-venous doses were given throughout the surgical and experimental procedures in order to maintain a deep level of anaesthesia. Following the performance of a conventional laminectomy from L4 to S1 and exposure of the sciatic nerve in the left hip, the animal was mounted in a rigid 'Goteborg' type spinal cord recording frame. Before initiating the intracellular recordings, the cats were paralysed with gallamine triethiodide and mechanically respired. Subsequently, the depth of anaesthesia was adjusted to maintain a stable blood pressure (monitored with a carotid artery cannula) below 120 mmHg, and to minimize or eliminate the appearance of spontaneous synaptic noise in the intracellular recordings. In addition, the animals were allowed frequent periods of recovery from paralysis to ensure the absence of withdrawal reflexes. We obtained intracellular recordings from cat lumbar motoneurones with 3 m KCl-filled micropipettes with tips broken to yield *in situ* resistances of 2–8 MΩ. Motoneurones were identified by antidromic activation following stimulation of the sciatic nerve. At the conclusion of the experiment, the animals were killed with a lethal dose of pentobarbitone.

Recording and current injection techniques

Motoneurones were initially accepted for study if they exhibited resting potentials more negative than −60 mV and action potentials with positive overshoots. We performed the complete experimental protocol only on those motoneurones capable of producing sustained, repetitive discharge in response to long suprathreshold current steps. We injected a series of current waveforms into the motoneurones in order to determine their input resistance, rheobase and steady-state frequency–current relation, as well as their response to white noise. The waveforms were stored as sequences of digitized values and converted to a current command via a D/A converter at a rate of 10 kHz. The membrane potential was simultaneously sampled at the same rate and stored. The membrane potential and injected current waveforms were also recorded on VCR tape using a PCM recording adapter (bandwidth, 0–22 kHz).

The current command waveform consisted of a series of discrete increments, each of which produced an artifact in the voltage

record associated with any uncompensated electrode capacitance and resistance. The residual electrode transient was estimated off-line by averaging and normalizing the initial response to a number of current steps. This average electrode transient was convolved with the stimulus waveform and then subtracted from the recorded membrane potential record (Poliakov et al. 1996). The occurrence times of the spikes were determined from the 'corrected' membrane potential trajectories and defined as the points of the highest positive slope of the spike waveform, i.e. the maximum of the derivative of the signal. From the averaged spike trajectories (see Fig. 4), we determined that the foot of the spike occurred 0·4–0·5 ms prior to the point of maximal slope.

Stimulus waveforms

The stimulus waveforms included different zero-mean random processes superimposed upon a long (39 s) suprathreshold current step. A brief series of subthreshold, 50 ms current pulses preceded and followed the suprathreshold stimulus and were used to calculate the input resistance, the electrode transients, and the time constant of the motoneurone (see below). The random processes lasted for 26·2 s (2^{18} samples at the 10 kHz sampling rate) and were added to the suprathreshold step 9 s after its onset. (This delay was chosen to minimize the spike-frequency adaptation that is largely complete at this time; cf. Sawczuk et al. 1995.) We used two different types of random processes: the first (current transient (CT) waveform) was constructed of trains of positive and negative current transients designed to mimic synaptic currents, whereas the second (white noise (WN) waveform) was constructed to approximate bandwidth-limited white noise.

To compose the CT waveform, we generated independent Poisson trains (mean interval, 25 ms) for each of ten excitatory and ten symmetric, inhibitory current transients, and then we added these trains together (Fig. 1*B*, upper trace). Using this waveform as a stimulus allowed us to study the modulation of firing rate in response to all twenty excitatory and inhibitory current transients by compiling PSTHs between each Poisson stimulus train and the motoneurone spike train. The individual current transients ($c_k(t)$: current amplitude as a function of time, t, for $k = 1$, 2, ... 20 different waveforms) were described by the α-function (Rall, 1967):

$$c_k(t) = a_k(t/\tau_k)\exp(1 - t/\tau_k), \tag{1}$$

where a_k is the amplitude and τ_k the rise time of the current transient. Figure 1*A* shows the twenty current transients used in the experiments on cat lumbar motoneurones. The absolute values of amplitude varied from 0·7 to 2·8 nA and values of rise time varied from 0·1 to 1·6 ms. These ranges permitted us to examine the effects of changes in the amplitude, rise time and polarity of current transients on the features of the PSTHs. For the rat experiments, the waveform was reduced elevenfold to account for the differences in input resistance between cat lumbar and rat hypoglossal motoneurones (see Results).

To implement the white noise method of system identification (Marmarelis & Marmarelis, 1978), we were required to generate another stimulus waveform that approximated bandwidth-limited white noise. The CT waveform, although a random process, does not meet the criteria of white noise, i.e. a Gaussian distribution of amplitudes and a flat power spectrum (Marmarelis & Marmarelis, 1978). The distribution of amplitudes of the CT waveform is too narrow (Fig. 1*C*, thick line), and its power spectrum shows a marked decline with increasing frequency (Fig. 1*D*, thick line). The CT waveform was modified to make waveform WN by adding an independent random process $y(t)$:

$$\mathrm{WN} = \mathrm{CT} + y(t). \tag{2}$$

The power spectrum of $y(t)$ (Fig. 1D, dotted line) compensated for the fall-off in power of the CT waveform at higher frequencies (see Appendix for details of the calculations). For the resulting WN waveform (Fig. 1B, lower trace), the amplitude probability density was Gaussian (Fig. 1C, thin line; mean = 0; s.d. = 2·5 nA) and the power spectrum was flat for frequencies up to 500 Hz (Fig. 1D, thin line). This waveform can be used to implement the white noise method (Marmarelis & Marmarelis, 1978), and since it contains the CT waveform, it can also be used to estimate the response of the

motoneurone to any individual current transient by compiling PSTHs of motoneurone discharges to the corresponding Poisson train.

Experimental protocol

The rheobase and steady-state frequency–current $(f-I)$ relation of each cell were determined prior to the application of the current transient (CT) and white noise (WN) waveforms. We injected 50 ms current steps of various amplitudes and determined the rheobase
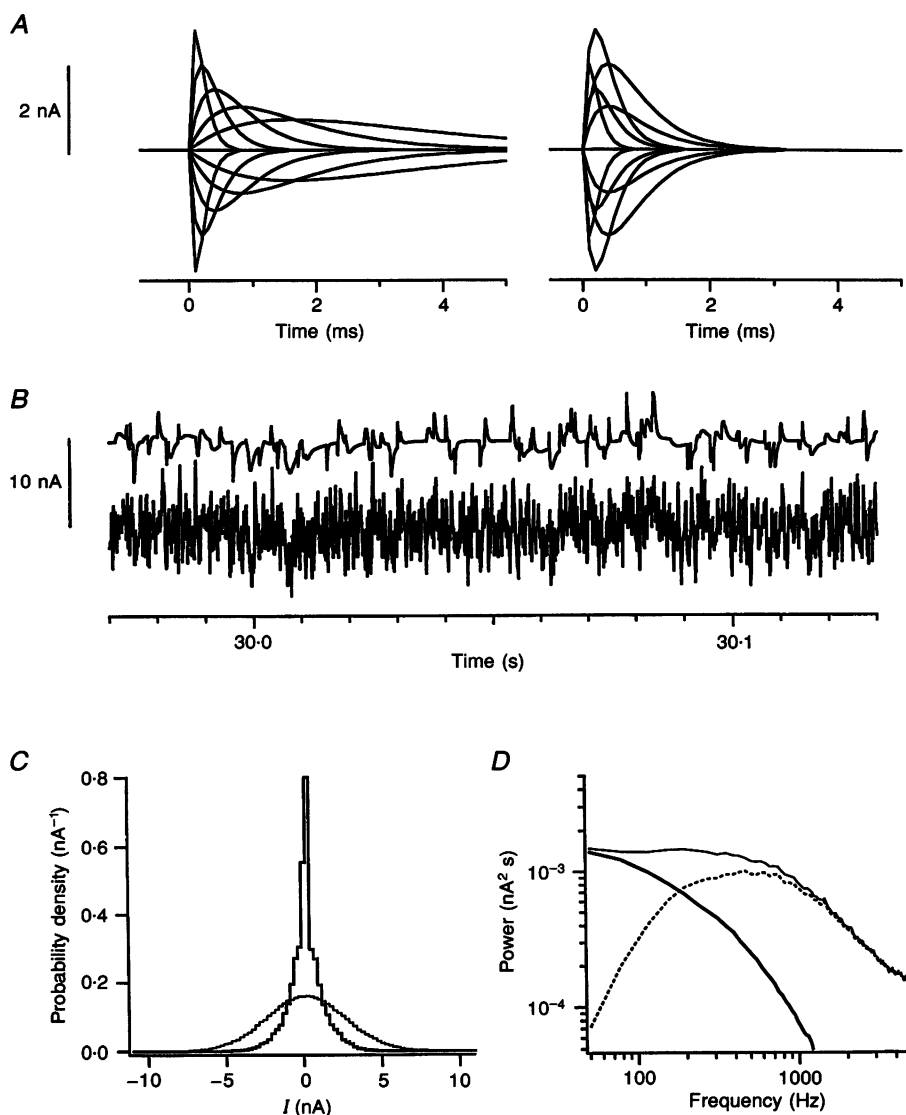
Figure 1. Composition of the current waveforms injected into the somata of cat lumbar motoneurones

A, the waveforms of 10 depolarizing and 10 symmetric hyperpolarizing current transients ($c_k(t)$, where $k = 1$, 2, ...20) used to generate the CT waveform. The individual transients were described by an α-function (cf. Methods, eqn (1)) with rise times ranging from 0·1 to 1·6 ms. B, sample records of the injected current waveforms (the traces have been offset for clarity). The upper trace shows the CT waveform composed of a sum of Poisson trains of the 20 current transients shown in A. The lower trace shows the white noise waveform (WN). C, probability density histograms for the amplitudes of the CT (thick trace) and WN (thin trace) waveforms. D, the power density spectra for the CT (thick trace) and WN (thin trace) waveforms. The CT waveform (upper trace in B) has a rapid fall-off in its power density as frequency increases. To obtain the WN waveform, an independent random process (dotted line) was added to the CT waveform (see Appendix). The power density of the composite waveform (WN) is flat up to nearly 500 Hz.

current as the minimum current amplitude needed to elicit a spike. The steady-state *f–I* relationship was estimated by delivering a series of 500 ms current steps of various amplitudes and plotting the relation between current amplitude and the average frequency calculated over the last four interspike intervals of the response. (The slope of the relation determined in this fashion may be slightly higher than that of the true steady-state relation; see Sawczuk *et al.* 1995.)

Two versions of each CT and WN stimulus waveform were applied. In the first, the appropriate zero-mean random process (CT or WN) was added to the suprathreshold current step and in the second, that same process was subtracted from the current step. The complete experimental protocol consisted of the following sequence of eight trials: +WN, −WN, +CT, −CT, −CT, +CT, −WN, +WN. The use of positive and negative versions of a given random waveform reduced any bias that might be introduced by repeating the same pseudo-random waveform several times. In addition, repeating the basic sequence of four waveforms in forward and then in reverse order helps compensate for any slow changes in cell properties that occur during the course of the entire protocol. Early on we found that the effect of a given current transient on firing probability was nearly identical in the CT and WN trials (see Results), so in many cells only the four WN trials were applied. After the initial set of four or eight trials, we re-measured the *f–I* relation, and in some motoneurones repeated the entire protocol after changing the amplitude of the underlying suprathreshold current step to alter the mean firing rate of the motoneurone.

Data analysis

We obtained a number of derived measures from the digitized membrane responses to the stimuli, including: (1) the profiles of the simulated PSPs, i.e. the subthreshold membrane potential responses of the motoneurone to each of the twenty current transients (CTs); (2) PSTHs between the times of occurrence of CTs and motoneurone spikes; and (3) zero-, first- and second-order Wiener kernels.

The recorded membrane potentials were first corrected for electrode artifacts as described earlier. Although this procedure facilitated accurate measurement of the times of spike occurrence, a significant contribution from uncompensated electrode resistance often remained in the records because of changes in electrode resistance during the course of a 40 s trial. For this reason, it was not possible to measure accurately the membrane potential response to a given current transient. Instead, we estimated the membrane response to each current transient using a parallel RC circuit model of the neurone. Each simulated PSP (i.e. the profile of the membrane potential induced by each CT) was reconstructed, using the input resistance of the motoneurone (R_N) and membrane time constant (τ_0) values. These values were derived from the average responses of the motoneurone to the series of 50 ms current pulses, which was included at the beginning and at the end of every trial. We estimated τ_0 from the best-fit exponential curve (curve-fitting routine of Igor Pro, Wavemetrics Inc., Lake Oswego, OR, USA) to the averaged membrane potential trajectory in response to the onset of the largest hyperpolarizing pulse. R_N was calculated as the slope of the relationship between the current pulse amplitude and the resulting change in the membrane potential measured at the end of the 50 ms current pulse.

Each of the twenty Poisson trains of CTs were used to compile a PSTH between the CT onset times and the times of the motoneurone spikes. PSTHs were calculated over lags of 50 ms

prior to and following the CT, using a bin width of 0·1 ms. The PSTHs were typically compiled from four or eight repetitions of the 26·2 s random input. Thus, there were typically either about 4200 or 8400 triggers used in each PSTH. The PSTHs had a range in average baseline counts per bin of 4 to 12 (for 4200 triggers) or 8 to 24 (8400 triggers), depending on the firing rate of the motoneurone. PSTH values, if normalized by the product of the bin width and the number of triggering events, represent the average instantaneous firing rate as a function of time from the onset of the CT stimulus.

Cumulative summations (CUSUMs; Ellaway, 1978) were calculated by subtracting the mean bin count at negative lags from the PSTH, and integrating the result. All of the CUSUMs had a defined maximum and were used to obtain the following quantitative characteristics of the PSTHs: peak area (over the baseline value), the mean percentage change in firing during the peak, and the peak duration. In the case of the PSTHs associated with hyper-polarizing current transients, analogous measurements were made on the PSTH trough. The peak area was obtained from the maximum value of the CUSUM, and the time at which this value was obtained was considered to be the end of the peak (Figs 2 and 3). The onset of the peak was taken as the fourth of seven consecutive CUSUM values at positive lags that were greater than zero. The peak duration is simply the difference between the peak onset and the end of the peak. The mean percentage change (MPC) in discharge rate is the same measure as the mean percentage increase described by Cope *et al.* (1987): MPC = peak area/peak duration, taken as a percentage of the background firing rate.

We used the response of the motoneurone to the WN waveform to implement the white noise method of system identification. Using this approach, the response of a system to any input is characterized by a series of Wiener kernels h_0, $h_1(\tau)$, $h_2(\tau_1,\tau_2)$, etc. of increasing order. In the case of a discrete output (i.e. the train of motoneurone discharges at times t_1, t_2, ... t_N), the kernels are easily estimated by the cross-correlation technique (see Lee & Schetzen, 1965; Bryant & Segundo, 1976; Marmarelis & Marmarelis, 1978) as follows:

$$h_0 = N/T, \tag{3a}$$

$$h_1(\tau) = h_0 P^{-1}\left(\sum_{i=0}^{N} w(t_i - \tau)/N\right), \tag{3b}$$

$$h_2(\tau_1,\tau_2) = h_0(2P^2)^{-1}\left(\sum_{i=0}^{N}(w(t_i - \tau_1)w(t_i - \tau_2) - a(\tau_1 - \tau_2))/N\right), \tag{3c}$$

etc.,

where w is the value of the input, t_i is the time of i-th discharge, N is the total number of discharges and T is the duration of neurone firing. P is the power of the input white noise signal and $a(\tau)$ is its autocorrelation function (derivations for both P and $a(\tau)$ for our signal WN are presented in the Appendix). The kernels in eqns (3b) and (3c) were estimated over intervals of ±50 ms.

The zero-order kernel, h_0, is a constant equivalent to the mean firing rate. The first-order kernel, $h_1(\tau)$, is estimated from the first-order cross-correlation between the input and the output. For a system with a discrete output, $h_1(\tau)$ becomes the spike-triggered average of the input signal, reversed in time and multiplied by the coefficient h_0/P. The second-order kernel, $h_2(\tau_1,\tau_2)$, is estimated from the second-order cross-correlation, and reflects the interaction between the two portions of the input signal in the past. A non-zero, second-order kernel is indicative of non-linear behaviour of the system.

In general, the response of the system, $Y(t)$, to an arbitrary input, $X(t)$, can be approximated as a sum of Wiener functionals, G_i:

$$Y(t) = G_0(t) + G_1(t) + G_2(t) + \text{etc.,} \qquad (4)$$

where

$$G_0(t) = h_0, \qquad (5a)$$

$$G_1(t) = \int_0^\infty h_1(\tau) X(t-\tau)\, d\tau, \qquad (5b)$$

$$G_2(t) = \iint_0^\infty h_2(\tau_1,\tau_2) X(t-\tau_1) X(t-\tau_2)\, d\tau_1 d\tau_2 - P\int_0^\infty h_2(\tau,\tau)\, d\tau, \qquad (5c)$$

etc.

The zero-order functional, $G_0(t)$, is a constant equal to the mean firing rate, h_0. The first-order functional, $G_1(t)$, is the convolution of the first-order kernel, $h_1(\tau)$, with the input, $X(t)$. The sum of these two terms is the best-fit approximation of the output of a linear system to a white noise input signal (Marmarelis & Marmarelis, 1978).

Higher-order Wiener functionals describe the deviation of the output $Y(t)$ from that of a linear system. We truncated the sum in eqn (4) at $G_2(t)$ because functionals of the third order and higher require rather intensive computations, the results of which are difficult to display and analyse. The second-order Wiener approximation (i.e. the sum $G_0(t) + G_1(t) + G_2(t)$) forms a non-linear analytical model of the system. It is the best-fit, second-order approximation of the system with respect to the white noise stimulus, and can be used to predict its response to any input within the noise. In order to predict the response of a motoneurone to a particular current transient $c_k(t)$, one has to substitute the input for $X(t)$ in eqns (5b) and (5c). Since $c_k(t) = 0$ for $0 > t > 20$ ms, the infinite integration limits in eqns (5b) and (5c) can be replaced with finite limits.

RESULTS

Motoneurone properties

The following analyses of the relation between injected current transients and the associated changes in motoneurone firing probability are based on *in vitro* recordings from seven rat hypoglossal motoneurones and *in vivo* recordings from three cat lumbar motoneurones. The rat hypoglossal motoneurones exhibited resting potentials ranging from -80 to -60 mV, input resistances from $9\cdot9$ to $26\cdot6$ MΩ (mean $\pm$ s.d. $= 17\cdot2 \pm 6\cdot1$ MΩ) and membrane time constants from $4\cdot6$ to $8\cdot8$ ms ($6\cdot4 \pm 1\cdot3$ ms). Their rheobases ranged from $0\cdot15$ to $0\cdot59$ nA ($0\cdot32 \pm 0\cdot14$ nA), and the slopes of their steady-state frequency–current (f–I) relations ranged from $12\cdot3$ to $28\cdot6$ impulses s^{-1} nA^{-1} ($20\cdot8 \pm 6\cdot2$ impulses s^{-1} nA^{-1}). These values are well within the range reported previously from this laboratory (Sawczuk *et al.* 1995; Poliakov *et al.* 1996), and agree with those reported by other investigators (Haddad *et al.* 1990; Viana *et al.* 1995; for discussion see Sawczuk *et al.* 1995). The resting membrane potentials for the three cat motoneurones were below -60 mV with positive action potential overshoots. The input resistances were $0\cdot95$, $1\cdot67$ and $1\cdot57$ MΩ and the membrane time constants were $5\cdot3$, $7\cdot0$ and $6\cdot3$ ms. The rheobases were $8\cdot5$, $3\cdot3$ and $8\cdot8$ nA, and the

the slopes of their steady-state f–I relations were $1\cdot2$, $1\cdot9$ and $1\cdot6$ impulses s^{-1} nA^{-1}. All of these values are consistent with those reported previously for cat lumbar motoneurones (reviewed in Binder, Heckman & Powers, 1996).

Membrane responses to current transients

As the current transients varied in amplitude and duration, the time courses of the induced simulated PSPs also varied. The time courses of simulated PSPs produced by the same current transient in different cells were somewhat different, depending on the input resistance and time constant of the particular cell. In both cat and rat motoneurones, the peak amplitudes of these simulated PSPs were similar and ranged from 79 to 660 μV. (Note that the current was reduced elevenfold for the rat motoneurones; see Methods.) Their rise times ranged from $0\cdot5$ to $5\cdot8$ ms. For comparison, the unitary excitatory PSPs produced by I a afferent fibres in cat lumbar motoneurones varied from 24 to 538 μV in amplitude, and their rise times ranged from $0\cdot2$ to $2\cdot1$ ms (Cope *et al.* 1987). Unitary IPSPs produced by I a reciprocal interneurons ranged from -25 to -215 μV in amplitude with the time to minimal value being of the order of 1 ms (Stuart & Redman, 1990). Therefore, the range of time courses of the simulated PSPs we induced with various current transients included those of naturally occurring excitatory and inhibitory PSPs, and their range of amplitudes were similar to those of unitary and small compound EPSPs and IPSPs.

## Relation between PSTH and simulated PSP features

Previous comparisons of PSTH features with the amplitudes and time courses of synaptic potentials have generally relied on pooling data from different cells or from sequential recordings in the same cell (Fetz & Gustafsson, 1983; Gustafsson & McCrea, 1984; Cope *et al.* 1987). The present results are unique in that comparisons can be made of PSTH and simulated PSP features over a wide range of PSP sizes and shapes applied in the same cell under identical conditions. The relationships between PSTH and PSP features for a given cell were therefore unaffected by variations in intrinsic cell properties or background synaptic noise.

PSTHs produced by a particular current transient were not significantly affected by the addition of high-frequency noise to the current waveform. As described in Methods, one current waveform, CT, was composed of current transients alone, whereas a waveform approximating white noise, WN, was obtained by adding an independent higher-frequency random process to the CT waveform. Although previous work in our laboratory (Poliakov *et al.* 1995) has indicated that PSTH features can be modified by the addition of noise, the CT waveform used in the present study was already quite noisy (cf. Fig. 1*B* and *D*), so that the further addition of another noise waveform, whose power was relatively small and limited to higher frequencies, did not noticeably affect the PSTH characteristics. For three rat motoneurones, we performed a regression analysis for the values of several PSTH parameters (peak amplitude, peak area and peak duration) obtained from responses to the CT and WN waveforms. The parameter values found for twenty current transients using the WN waveform were plotted

against the corresponding values found for the CT waveform, and regression lines were fitted to these plots. For each of the three motoneurones, the best-fit regression lines were not statistically different from the line of identity (the intercept values were not different from 0 and the slope values were not different from 1; $P > 0.05$). When the data from the three motoneurones were pooled, the slope values of the fitted lines were 0·99 for peak amplitude and 1·02 for peak area.

The histograms in Fig. 2A represent the PSTHs compiled from the onset times of a depolarizing (top traces) and a symmetric hyperpolarizing (bottom traces) current transient in a cat motoneurone. The current transients (thick traces) and their associated PSPs (dashed traces) are shown directly below the PSTHs. The most prominent PSTH features are a short-latency peak in response to the depolarizing current transient and a short-latency trough in response to the

hyperpolarizing current transient. Both the areas of the PSTH peaks (and troughs) and the mean changes in firing rates were well correlated with the estimated PSP amplitude. Figure 2B and C illustrate the relationships between these two different PSTH measures and estimated PSP amplitudes for the responses to all twenty current transients in the same cat motoneurone. For all of the motoneurones, the slope of the relation between PSTH peak area and PSP amplitude (Fig. 2B) was always greater for depolarizing than for hyperpolarizing PSPs. In the rat motoneurones, the corresponding slopes ranged from 0·09 to 0·49 extra impulses per millivolt (0.25 ± 0.13) for depolarizing PSPs and 0·04 to 0·21 fewer impulses per millivolt (0.14 ± 0.06) for hyperpolarizing PSPs. In the cat motoneurones, the corresponding slopes ranged from 0·13 to 0·14 extra impulses per millivolt (0.13 ± 0.01) for
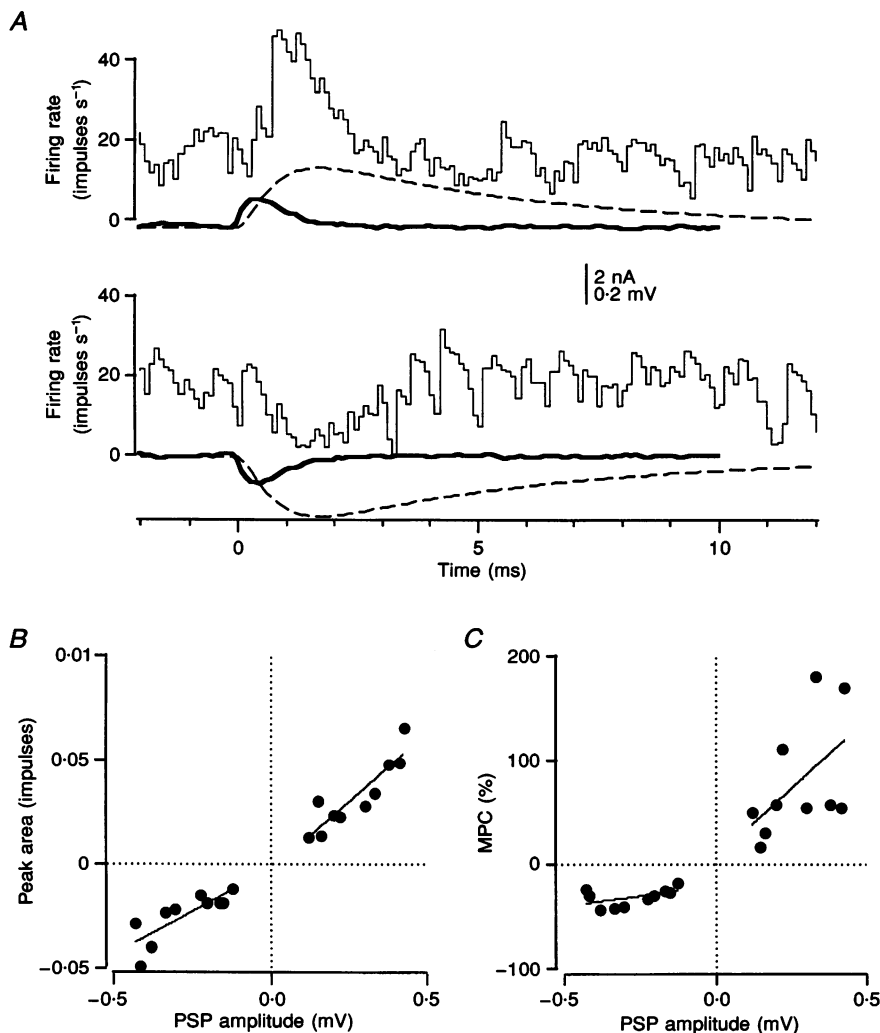
Figure 2. Responses of a cat lumbar motoneurone to depolarizing and hyperpolarizing injected current transients

A, symmetric injected depolarizing (top) and hyperpolarizing (bottom) current transients (thick lines) produced asymmetric PSTHs. The dashed lines show the estimated changes in membrane potential (simulated PSPs) induced by the current transients. B, PSTH peak area plotted as a function of the amplitude of the PSP evoked in the motoneurone. The lines are the best-fit linear regressions calculated separately for depolarizing and hyperpolarizing PSPs. C, mean percentage change (MPC) in motoneurone firing rate produced by the PSPs plotted as a function of their amplitude.

depolarizing PSPs and 0·07 to 0·10 fewer impulses per millivolt (0·09 ± 0·02) for hyperpolarizing PSPs. The difference in slope values for depolarizing and hyperpolarizing current transients indicates that the overall relationship is non-linear.

Similar non-linearities were observed for the relationship between the mean percentage change (MPC) in firing rate and PSP amplitude (Fig. 2C) and between the PSTH peak amplitude and PSP amplitude (not shown). For the data illustrated in Fig. 2C, the slope of the relationship between MPC and PSP amplitude was 0·27 % μV^{-1} for depolarizing inputs and 0·04 % μV^{-1} for hyperpolarizing inputs. Similar differences were observed for the other two cat motoneurones (the slopes for depolarizing inputs were 0·48 and 0·25 % μV^{-1}, whereas the slopes for hyperpolarizing inputs were 0·06 and 0·11 % μV^{-1}). The relationship between MPC and PSP amplitude was more variable in the rat motoneurones, but on average the slope for depolarizing inputs was about twice that for hyperpolarizing inputs (0·25 ± 0·13 % μV^{-1} and 0·13 ± 0·05 % μV^{-1}, respectively). For depolarizing inputs alone, the slopes of the linear fits between MPC and PSP amplitude for the present data are comparable to those of Cope et al. (1987), who reported a slope of 0·30 % μV^{-1} between mean percentage increase in firing rate and EPSP amplitude for their well-studied single I a fibre connections.

The slope values for the relationships between PSP amplitude and PSTH parameters depend upon our estimates of PSP amplitude. Since rat hypoglossal motoneurones are relatively compact electrotonically (Viana, Bayliss & Berger, 1994), our use of a single time constant approximation of the passive membrane response is probably justified. However, the passive impulse response of cat motoneurones is better approximated as the sum of at least two exponential terms (cf. Rall, 1969). In two of the three cat motoneurones, we averaged the membrane response to more than thirty repetitions of a brief (0·5 ms) hyperpolarizing current pulse, and were able to fit the membrane response with the sum of two exponential terms. Convolving this more realistic impulse response with the injected current waveforms led to larger predicted PSP amplitudes than those obtained with the single exponential impulse response. Nonetheless, in each cell the PSP amplitudes obtained by two different impulse responses were highly correlated ($r > 0.99$), so that the basic form of the relationships between PSTH and PSP parameters was not affected by the method used to predict the PSPs. Moreover, the non-linear relationships between the magnitude of the 'synaptic' input and PSTH parameters were also obtained when the area of the current transient was used as the independent variable.

Fetz & Gustafsson (1983) developed a simple threshold-crossing motoneurone model which predicts that the PSTH profile produced by an EPSP is a scaled version of the PSP derivative. We found, however, that the peak PSTH values were only weakly correlated with the peak derivative values (for depolarizing currents, the correlation coefficients were $r = 0.08 \pm 0.23$ in rat motoneurones and $r = 0.30 \pm 0.12$ in cat motoneurones). In all cat and rat neurones, we found that the duration of the PSTH peak was always longer than

the PSP rise time. This is in agreement with the previous studies, in which both unitary PSPs (Cope et al. 1987) and small compound PSPs (Knox & Poppele, 1977; Kirkwood & Sears, 1978; Fetz & Gustafsson, 1983) yielded PSTH peaks that were wider than the PSP derivative. On the other hand, it is clear from Fig. 2A that the duration of the PSTH peak (or trough) is clearly shorter than the underlying PSP, suggesting that the PSTH peak cannot be well approximated by a scaled version of the PSP itself (Moore et al. 1970).

Kirkwood & Sears (1978) suggested that the fit may be improved if the PSTH profile is approximated as a weighted, linear sum of the PSP profile and its derivative:

$$f(t) - f_0 = a\,e(t) + b\,de(t)/dt, \tag{6}$$

where a and b are constants and $e(t)$ and $de(t)/dt$ are the time courses of the PSP and its derivative, respectively. Although this formulation was originally intended to apply to unitary EPSPs with amplitudes in the order of 100 μV or less (Kirkwood & Sears, 1978), other investigators have applied this expression to the analysis of PSTHs produced by large unitary EPSPs (Cope et al. 1987) as well as compound EPSPs and IPSPs (Gustaffson & McCrea, 1984). The range of simulated PSPs produced in our motoneurones allowed us to test the extent to which this formula could provide a general fit to PSTHs associated with large unitary and small compound PSPs. We calculated the best match to individual PSTHs using this approximation (curve-fitting routine of Igor Pro). Figure 3A shows the PSTHs compiled for four different depolarizing current transients injected into single cat (left column) and rat (right column) motoneurones. The current transients are illustrated by the continuous thick lines beneath each PSTH and the resultant PSPs are represented by dashed lines. The smooth, continuous traces superimposed on the histograms represent the best fit to each PSTH (see legend for details of the fitting procedure). The matches are quite good for the slower current transients (bottom four panels), but tend to underestimate the duration of the PSTH peak (or trough) for the faster current transients. This difference between predicted and observed PSTH time course in response to rapid current transients was more marked in rat motoneurones, which tended to have wider PSTH peaks than cat motoneurones. Moreover, the values of the fitting coefficients a and b were not constant for different inputs studied in the same motoneurone.

Figure 3B illustrates the relationships between the values of the coefficients and the PSP times to peak for all of the depolarizing and hyperpolarizing transients. The left graph corresponds to the cat motoneurone and the right graph to the rat motoneurone. In all cases, the contribution of the PSP derivative to the overall shape of the correlogram is much greater than that of the PSP itself. (In our eqn (6), $de(t)/dt$ is scaled in mV s^{-1}, so that the correlogram value can be expressed directly in impulses s^{-1}. The value of the

fitting coefficient b would be a thousandfold larger if the PSP derivative were expressed in mV ms^{-1} (cf. Kirkwood & Sears, 1978; Gustaffson & McCrea, 1984).) The scaling factor for the contribution of PSP derivative to the PSTH profile

(coefficient b) increased with the PSP time to peak and tended to be higher for depolarizing than for hyperpolarizing inputs. Similar findings were obtained in all of the other motoneurones.
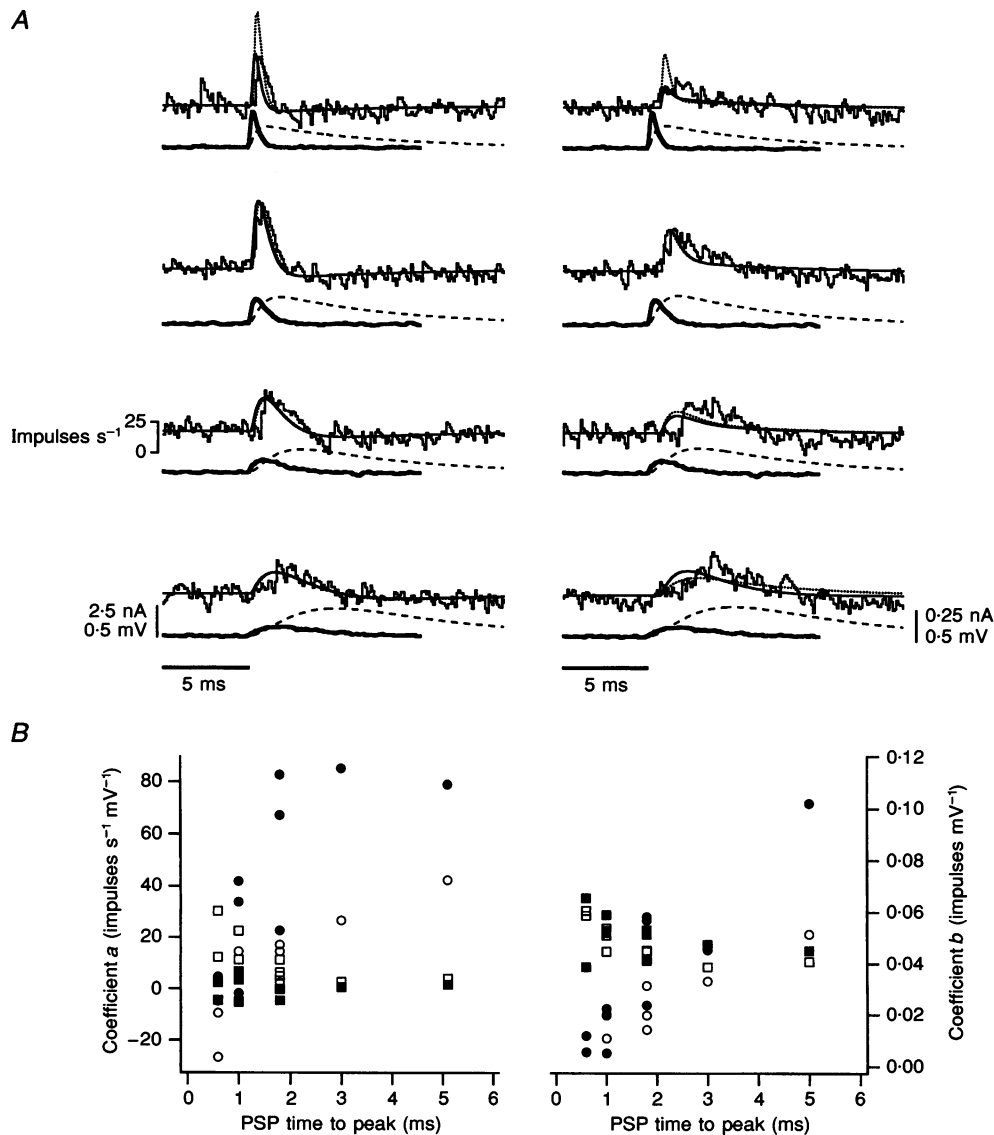

Figure 3. Matching PSTH profiles with the underlying PSP and its derivative

A, the responses of a cat lumbar motoneurone (left column) and rat hypoglossal motoneurone (right column) to four different excitatory current transients (continuous thick lines below PSTHs). The time to peak values of the transients were 0·2, 0·4, 0·8 and 1·6 ms. The continuous lines fitted to the PSTHs show the best-fit approximation using a combination of the evoked PSP waveform, $e(t)$, and its derivative, $de(t)/dt$. (Change in firing rate $= f(t) - f_0 = ae(t) + bde(t)/dt$.) The PSP waveforms (dashed lines below PSTHs) were calculated as described in Methods. The onset of the increase in firing probability in the PSTH occurs after time zero. The value of this onset delay was determined by first averaging the PSTHs in response to the 8 largest depolarizing transients and then determining the first of 7 bin values that exceeded the mean baseline discharge rate by at least 30%. Each PSP was then time shifted by this amount before determining the values of a and b in eqn (6) that gave the best fit to the PSTH. The dotted lines superimposed on the PSTHs show the results when coefficients a and b were fixed at the values that gave the best fit to one of the PSTHs (the second from the top). *B*, best-fit values for coefficients a (left axis, squares) and b (right axis, circles) for all 20 current transients in the cat (left graph) and rat (right graph) motoneurones. Depolarizing transients are denoted by filled symbols; hyperpolarizing transients by open symbols.

These results indicate that although individual PSTH profiles can often be well approximated by a linear combination of the underlying PSP and its derivative, this approximation does not provide a good *general* description of the characteristics of a synaptic input and its effects on motoneurone firing probability. Were it to do so, the values of the fitting coefficients would have to be constant for a particular motoneurone. The dotted lines superimposed on the PSTHs in response to the depolarizing current transients represent the fits of eqn (6) when the values of a and b are fixed at those which give the best fit to the second PSTH from the top in each column. It is clear that this approximation provides a poor fit to the PSTHs produced by the briefest current transients (the top of each column). In the following sections, we describe the use of the white noise method to derive a more general linear model.

White noise analysis: average current trajectory and membrane potential trajectory

The first step in constructing a general linear model of the input–output transform of motoneurones using a white noise input signal is to calculate the average spike-evoking current trajectory (ACT; Bryant & Segundo, 1976). Figure 4 presents the ACTs (upper traces) and the average membrane potential trajectories (lower traces) in a rat (A) and a cat (B) motoneurone. The pair of horizontal lines superimposed on each ACT represent the 96% confidence limits for the deviation of the current values from the mean current expected by chance alone (calculated as the mean $\pm$ 2 s.e.m., see Bryant & Segundo, 1976). The ACTs followed the same general pattern in all motoneurones studied: they first slowly declined below the mean current value. This prolonged shallow trough was followed by a peak just
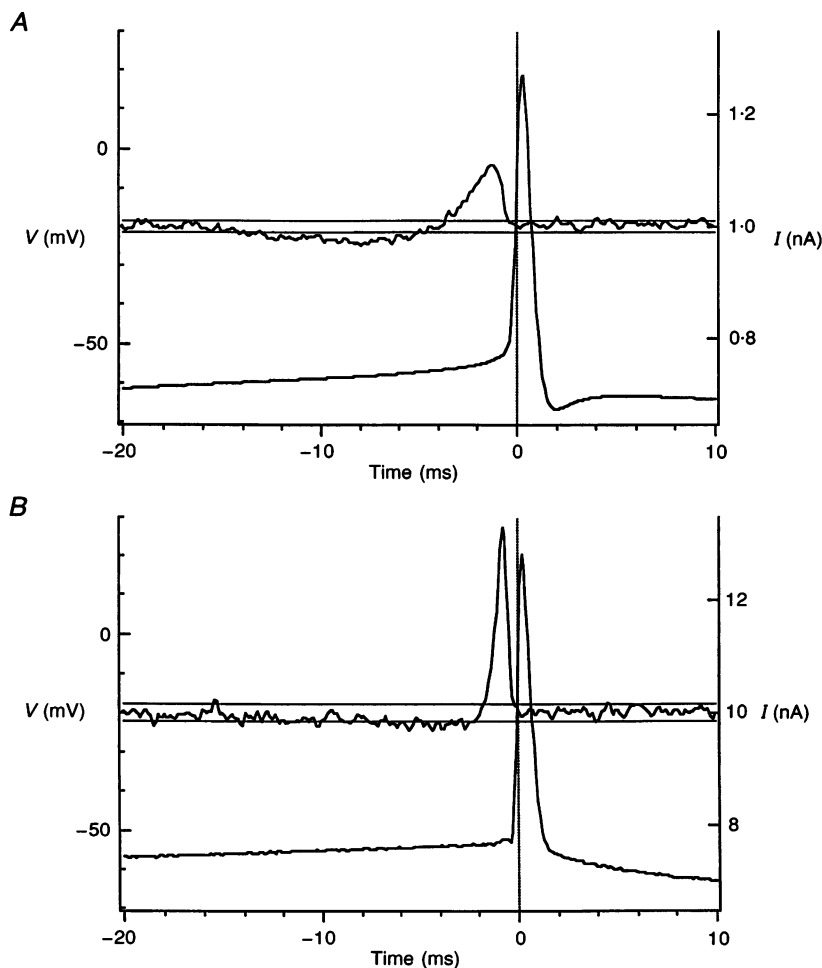

Figure 4. Action potentials and average spike-evoking current waveforms for rat and cat motoneurones in response to the white noise input

A, the lower trace shows the average membrane potential trajectory before, during and after action potentials in a rat hypoglossal motoneurone. The average spike-evoking current trajectory is shown in the upper trace. The average was computed from 4 trials of stimulation with white noise. The horizontal lines indicate 96% confidence limits for deviation of the average current trajectory from the mean current value. B, same display as in A, but for a cat lumbar motoneurone. Note the 10-fold difference in the current scale.

preceding the discharge, and then the ACTs returned to the level corresponding to the mean current value. Although the general pattern of the ACT is the same in rat hypoglossal (Fig. 4*A*) and cat lumbar (Fig. 4*B*) motoneurones, both the magnitude and time course of the trajectories differed in the two types of cells. A quantitative analysis of the differences in the responses of rat and cat motoneurones to the white noise input is presented below.

The profiles of the Wiener kernels

The first-order Wiener kernel is closely related to the averaged current trajectory. It is obtained by reversing the ACT in time and normalizing the resultant waveform by the ratio of the mean firing rate to the power of the noise stimulus (eqn (3*b*)). The first-order kernel, $h_1(\tau)$, obtained in a rat motoneurone is shown in Fig. 5*A*. The first-order kernel represents the changes in firing rate elicited by a
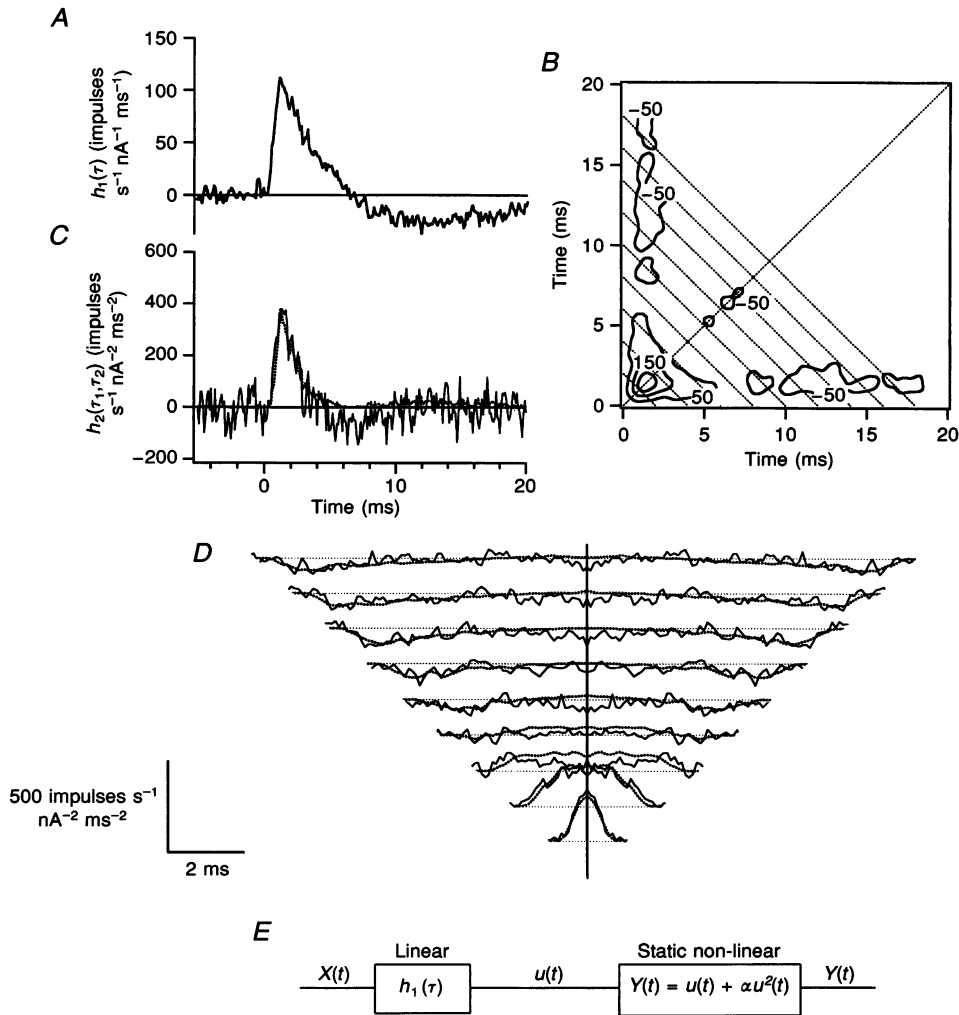
Figure 5. The input–output transform of a rat hypoglossal motoneurone identified by the white noise method

A, the first-order Wiener kernel, $h_1(\tau)$, depicts the linear impulse response of the neurone to a brief pulse of current (area, 1 nA ms). *B*, contour plot of the second-order Wiener kernel, $h_2(\tau_1,\tau_2)$, at levels −50, 50, 150 and 250 impulses s^{-1} nA^{-2} ms^{-2}. (Kernel values were smoothed before plotting using a two-dimensional, three-point smoothing routine: each plotted point represents the average of a three-by-three grid of the raw values.) Dotted lines are shown to define the dissections of the kernel, shown in *C* and *D*. *C*, the dissection of the second-order kernel, $h_2(\tau_1,\tau_2)$, along its main diagonal (i.e. $\tau_1 = \tau_2$). The superimposed dotted line shows the approximation of the second-order kernel as described by eqn (10) in the text: $\alpha h_1(\tau)h_1(\tau)$. *D*, the family of functions $h_2(\tau_1,\Theta - \tau_2)$ is shown by the continuous lines. These represent the dissections of the second-order Wiener kernel perpendicular to the main diagonal for $\tau_1 = \Theta - \tau_2$, with $\Theta = 2, 4, 6, 8, 10, 12, 14, 16, 18$ ms, increasing from bottom to top. The thick dotted lines show the functions given with the second-order kernel approximation: $\alpha h_1(\tau_1)h_1(\tau_2)$. The zero level for each function is shown by the thin dotted lines. *E*, the input–output function of the neurone can be represented as a second-order Wiener model: a cascade of a dynamic, linear transform described by the first kernel $h_1(\tau)$, followed by a static non-linearity.

brief pulse of current whose area is 1 nA ms. Like the ACT from which it was calculated, $h_1(\tau)$ consists of two phases: an initial sharp increase in firing rate, followed by a shallower but more prolonged decrease in firing rate. For our sample of seven rat hypoglossal motoneurones recorded under the same experimental conditions (i.e. motoneurone firing in response to the WN waveform superimposed onto 0·9 nA step of current, which produced tonic firing at rates of $16·5 \pm 4·3$ impulses s^{-1}), we found similar kernel profiles with the following characteristics: the peak amplitude of the positive phase ranged from 106·7 to 200·9 impulses s^{-1} nA^{-1} ms^{-1} (mean: 144·4 $\pm$ 34·7 impulses s^{-1} nA^{-1} ms^{-1}); the time to peak ranged from 1·1 to 2·0 ms (mean: 1·50 $\pm$ 0·32 ms);   the peak   area   ranged   from   218·6   to 349·9 impulses s^{-1} nA^{-1} (mean: 291·6 $\pm$ 50·3 impulses s^{-1} nA^{-1}); and the peak duration ranged from 3·1 to 6·6 ms (mean: 5·0 $\pm$ 1·2 ms). The convolution of the first-order kernel with the input gives the best-fit, linear model of the system under these conditions (Marmarelis & Marmarelis, 1978). If the input signal is small and the system exhibits near-linear behaviour, this model accurately predicts the output. In particular, if the input is a brief pulse of area A at time 0, the system response $(r(t))$ is well approximated by the following function:

$$r(t) = h_0 + A h_1(\tau). \qquad (7)$$

The second-order Wiener kernel, $h_2(\tau_1,\tau_2)$, is calculated by a second-order cross-correlation between the motoneurone spikes and the input signal at two different time lags (τ_1 and τ_2, see eqn (3c)). The result is a function of two variables (τ_1 and τ_2) and is symmetric with respect to the main diagonal $\tau_1 = \tau_2$. In Fig. 5B we show a contour plot of the second-order kernel for the same rat motoneurone shown in Fig. 5A. The prominent features of this kernel are a peak with a maximal value at the point $\tau_1 = \tau_2 = 2·0$ ms and two symmetric depressions at lags of about 8–18 ms along the lines $\tau_1 = 2·0$ ms and $\tau_2 = 2·0$ ms. The second-order kernel describes the deviation of the output from that predicted by the first-order model (eqn (7)). The second-order prediction of the system response $r(t)$ to a brief pulse of area A at time 0 is:

$$r(t) = h_0 + A h_1(\tau) + 2A^2 h_2(\tau,\tau), \qquad (8)$$

where $h_2(\tau,\tau)$ represents the values of the second-order kernel along the main diagonal (this dissection is shown in Fig. 5C), and the term $2A^2 h_2(\tau,\tau)$ represents the deviation from linearity. Unlike the first-order model, this expression gives asymmetric responses to positive and negative pulses, because the coeffient $2A^2$ is positive in both cases.

For positive pulses, the response amplitude and area would increase in a greater than linear fashion with respect to A. For negative pulses, the response amplitude and area will decline less than linearly, reach a minimum, and start increasing. Thus, the short-latency, positive peak in the second-order kernel represents rectification of the input signal. As a result, the second-order Wiener model does not

predict the erroneous negative response values for large hyperpolarizing inputs, as does the first-order model (see Fig. 8A).

The depressions in the contour plot of the second-order kernel represent non-linear interactions between inputs occurring at different times. For example, the responses of a motoneurone to a pair of identical pulses separated by 10 ms differs from the linear sum of the effects of each pulse acting in isolation. The response $r(t)$ can be expressed as follows:

$$r(t) = h_0 + h_1(\tau) + h_1(\tau - 10) + 2A^2 h_2(\tau,\tau - 10), \qquad (9)$$

where $h_0 + h_1(\tau) + h_1(\tau - 10)$ is the response of a linear system to a pair of identical pulses at times 0 and 10 ms and the term $2A^2 h_2(\tau,\tau - 10)$ represents deviations from this sum due to non-linear interaction between the pulses. The interaction effects can be predicted from a kernel 'dissection' along a line starting at a point 10 ms along either the τ_1 or τ_2 axis, and running parallel to the main diagonal. Since this line crosses the 'depression zone' of the contour plot, the second-order Wiener model predicts that the response to the second pulse will be smaller than that to the first, as has been described in the experiments reported by Fetz & Gustafsson (1983).

The peak along the main diagonal of the second-order kernel occurs at about the same latency as the peak in the first-order kernel, whereas the symmetric depressions off the main diagonal occur at lags corresponding to the duration of the trough in the first-order kernel. This suggested to us that the second-order kernel might be approximated by a scaled version of the product of the values of the first-order kernel at delays τ_1, τ_2:

$$h_2(\tau_1,\tau_2) \approx \alpha h_1(\tau_1) h_1(\tau_2), \qquad (10)$$

where α is the scaling coefficient. As seen from formula (10), the units for this coefficient are seconds. We estimated the value of the coefficient by substituting the maximal values of the first- and second-order kernels into eqn (10). The accuracy of this approximation is illustrated in Fig. 5C and D. Figure 5C illustrates the 'dissection' of the second-order kernel contour plot along its main diagonal and Fig. 5D illustrates a family of 'dissections' perpendicular to the main diagonal. The continuous lines represent the actual values of the kernel (calculated from eqn (3c)) whereas the dotted lines represent the approximation of the second-order kernel based on eqn (10). As can be seen from Fig. 5D, the approximated and calculated kernel values are generally quite close, although the approximation does not account for the small depression along the main diagonal at lags of 10–15 ms. This form of the second-order kernel is characteristic of a system consisting of a cascade of a dynamic, linear component followed by a static non-linear component (Marmarelis & Marmarelis, 1978; Hunter & Korenberg, 1986). This so-called 'Wiener cascade model' (Sakai, 1992) is shown schematically in Fig. 5E.

The response of such a system $(Y(t))$ to any input $X(t - \tau)$ can be predicted as follows:

$$u(t) = \int_0^\infty h_1(\tau)X(t - \tau)\,d\tau, \tag{11a}$$

$$Y(t) = h_0 + u(t) + \alpha u^2(t). \tag{11b}$$

According to this Wiener cascade model, the input $X(t)$ is first convolved with the kernel $h_1(t)$ to produce an intermediate variable, $u(t)$, an operation known as dynamic, linear filtering (eqn (11a)). The output value, $Y(t)$, is then computed from the intermediate variable, $u(t)$, using a parabolic transform (eqn (11b)). This type of function is known as a static non-linearity because the output value is computed from the intermediate value at only a single moment in time. The static non-linearity can be described by this parabolic function, or some other function, as long as

its value, and its first and second derivative match those of the parabolic function over the range of interest.

For cat lumbar motoneurones, the characteristics of the transform of injected current into motoneurone firing were qualitatively similar to those of the rat hypoglossal motoneurones. Figure 6 shows the results found in one cat lumbar motoneurone. The kernels are presented in the same form as those for rat hypoglossal motoneurone in Fig. 5 (but note the difference in the time scale). In each of three cat motoneurones, we recorded firing in response to several different values of depolarizing current with the same WN waveform superimposed. The first-order Wiener kernels found for seven different trials performed in these three cat motoneurones exhibited the following characteristics: the peak amplitudes ranged from $19 \cdot 2$ to $57 \cdot 3$ impulses $s^{-1}\,nA^{-1}\,ms^{-1}$ (mean: $31 \cdot 7 \pm 13 \cdot 1$ impulses $s^{-1}\,nA^{-1}\,ms^{-1}$);
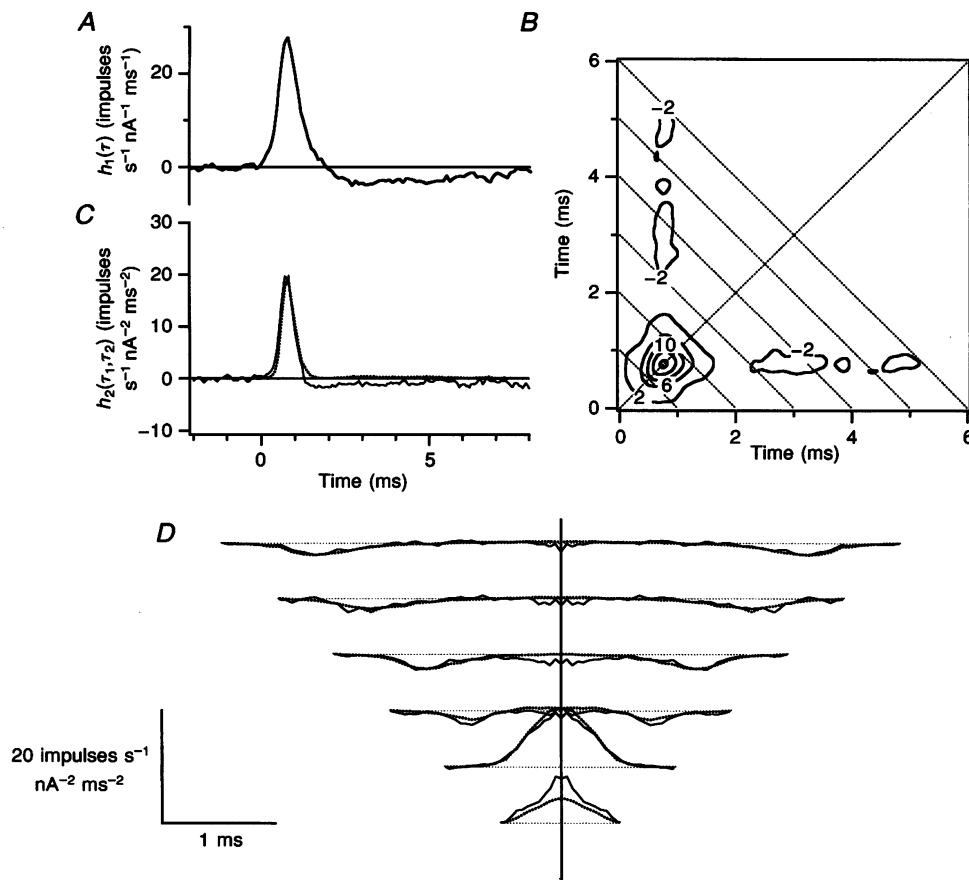

Figure 6. The input–output transform of a cat lumbar motoneurone identified by the white noise method

A, the first-order Wiener kernel, $h_1(\tau)$. *B*, contour plot of the second-order Wiener kernel $h_2(\tau_1,\tau_2)$ at levels -2, 2, 4, 6, 10, 14 and 18 impulses $s^{-1}\,nA^{-2}\,ms^{-2}$. Dotted lines are shown to define the dissections of the kernel, shown in *C* and *D*. *C*, the second-order kernel is shown by the continuous line. This is compared with an approximation of the second-order kernel, $\alpha h_1(\tau)h_1(\tau)$, shown by the dotted line ($\alpha = 0 \cdot 025$ s). *D*, the family of functions $h_2(\tau_1,\Theta - \tau_2)$ is shown by the continuous lines. These represent the dissections of the second-order kernel perpendicular to the main diagonal for $\tau_1 = \Theta - \tau_2$, with $\Theta = 1$, 2, 3, 4, 5, 6 ms increasing from bottom to top. The thick dotted lines show the functions given with the approximation of the second-order kernel, $\alpha h_1(\tau_1)h_1(\tau_2)$.

the time to peak ranged from 0·6 to 0·8 ms (mean: 0·63 ± 0·08 ms); the peak area ranged from 13·5 to 40·2 impulses s^{-1} nA^{-1} (mean: 22·3 ± 8·8 impulses s^{-1} nA^{-1}); and the peak duration ranged from 1·2 to 1·9 ms (mean: 1·5 ± 0·23 ms). Compared with rat motoneurones firing at comparable rates, the kernels found in cat motoneurones were about four times smaller in amplitude and about three times shorter in duration.

Similar to rat motoneurones, the relationship between the first- and second-order kernels in cat motoneurones could be well approximated by eqn (10), suggesting that the overall input–output transform can be represented as a cascade of a dynamic linear filter followed by a static non-linearity (eqns (11*a*) and (11*b*)). However, as was the case for rat motoneurones, this Wiener cascade model does not describe the measured second-order kernels precisely. In both types
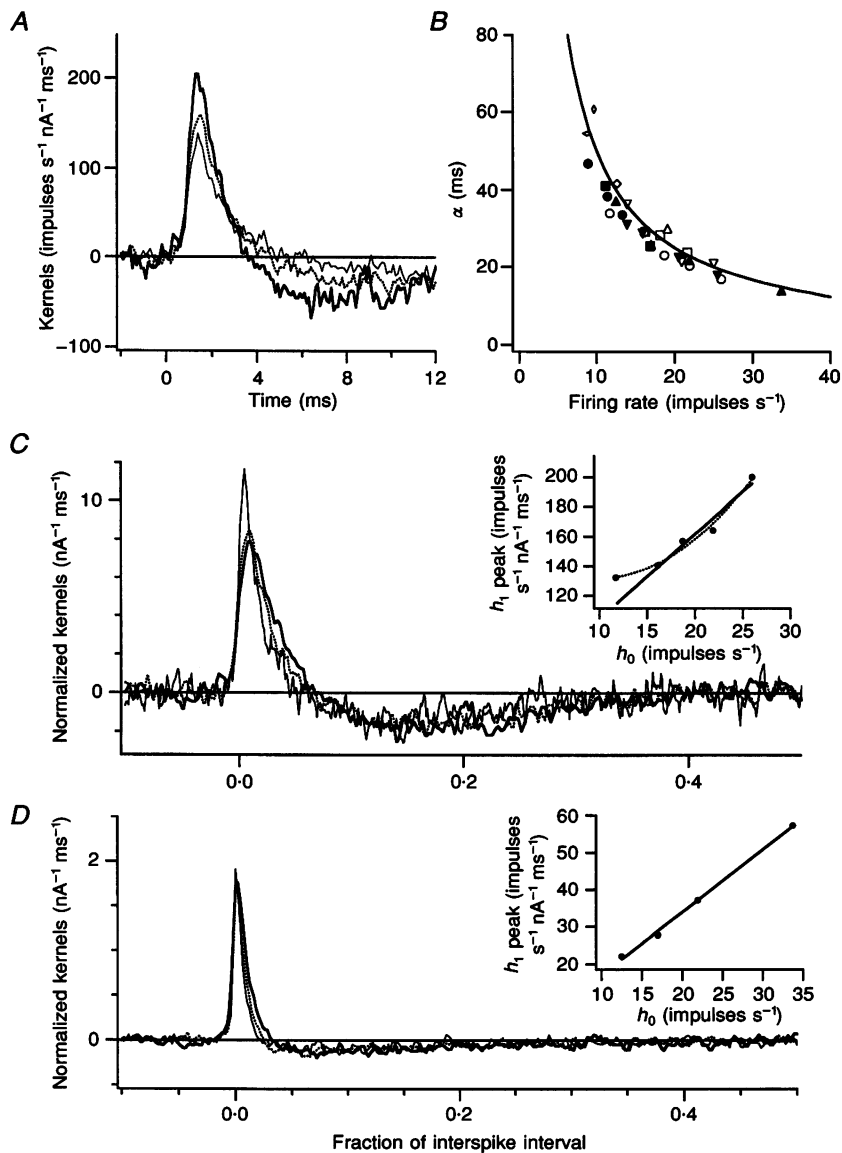
Figure 7. The effect of motoneurone discharge rate on the input–output function

A, the first-order Wiener kernels, $h_1(\tau)$, calculated at three different firing rates in the same rat hypoglossal motoneurone (12 impulses s^{-1}, thin line; 19 impulses s^{-1}, dotted line; 26 impulses s^{-1}, thick line). *B*, relationship between α, the coefficient determining the contribution of the second-order non-linearity to the input–output transform (eqn (11*b*) in the text), and h_0, the mean firing rate. Filled symbols represent cat spinal motoneurones, open symbols represent rat hypoglossal motoneurones. Different symbols represent different motoneurones. A hyperbolic function, $\alpha = 0·45$/firing rate fitted to these points is shown with the continuous line. *C*, the first-order Wiener kernels of *A* presented in normalized form. The time scale was normalized by the duration of the interspike interval and the amplitude scale was normalized by h_0, the mean firing rate. The inset shows the relation between h_0 and the peak amplitude of h_1 for the kernels illustrated in *A* and *C* as well as the kernels calculated at two other background rates. *D*, same as *C*, but for a cat lumbar motoneurone.

of motoneurones, the dissection of the second-order kernel along the main diagonal (Fig. 5C and 6C) is characterized by an initial peak followed by a shallow trough, which reaches negative values. In contrast, the values predicted by eqn (10) along the main diagonal are $\alpha h_1^2(\tau_1)$, an expression that cannot generate negative values.

Effects of motoneurone firing rate on input–output transform

We studied the effects of mean firing rate on the description of the input–output transform in three rat and three cat motoneurones. As described in Methods, the firing rate was varied by changing the amplitude of the depolarizing current step. Figure 7A shows the profiles of the first-order kernel $h_1(\tau)$ obtained in the same rat motoneurone at three different firing rates. At higher firing rates, the peak values of the first-order kernels increased, while the duration of the peak decreased. The relationship between the kernel profile and the background firing rate can be seen more clearly when the amplitude and time course of the kernels are normalized by firing rate as shown in Fig. 7C. The amplitudes of the kernel values were divided by the mean background firing rate and the time scale is presented as a fraction of the interspike interval. Figure 7D presents analogous normalized first-order kernels obtained from a cat motoneurone firing at three different background rates. The insets in Fig. 7C and D illustrate the relationship between the mean firing rate (h_0) and peak first-order kernel amplitudes for all of the firing rates studied in these two cells. With the exception of the lowest firing rate in the illustrated rat motoneurone, the peak first-order kernel amplitude grows linearly with increasing firing rate. The kernel profiles found for rat motoneurones (Fig. 7C) *in vitro* were significantly wider then those of cat motoneurones (Fig. 7D) recorded *in vivo*. However, for both types of cell, normalization revealed that the durations of both the peak and trough of the first-order kernels are inversely proportional to firing rate.

The relative contributions of the first- and second-order Wiener kernels to the overall transform can be estimated by comparing the values of the second and third terms in eqn (11b) ($u(t)$ and $\alpha u^2(t)$, respectively). The second-order contribution depends both on the value of $u(t)$ and on the value of the scaling coefficient, α. In Fig. 7B, the values of coefficient α are shown as a function of the mean firing rate for all rat (open symbols) and cat (filled symbols) motoneurones. The continuous line in the figure represents the best-fit, hyperbolic function, $\alpha = 0.45/\text{firing rate}$. Remarkably, α values measured in both cat and rat motoneurones, and in the same motoneurone at different firing rates, followed this hyperbolic function quite closely. Thus, the profile of the second-order kernel can be accurately predicted from the first-order kernel and the mean firing rate. Since the contribution of the linear component ($u(t)$) increases proportionally with firing rate, the term $u^2(t)$ increases with the square of firing rate. The inverse relationship between α and the mean firing rate

indicates that the amplitudes of both the linear and non-linear terms increase proportionally with firing rate so that to a first approximation their relative contributions are independent of firing rate. However, in Fig. 7C the normalized peak is highest at the lowest background firing rate, indicating that the relative contribution of the non-linear component would be somewhat higher at the lowest firing rate.

We have previously reported that the addition of white noise to a constant current step increases the mean firing rate of both cat and rat motoneurones (Poliakov *et al.* 1996). Since the white noise signal has a zero mean amplitude, the increase in motoneurone firing that it induces is a reflection of higher order non-linearities which are subsumed by the zero-order kernel, h_0 (cf. Moore & Auriemma, 1985). We estimated the effects of the noise stimulus on firing rate by comparing the mean firing rate during the period of noise application to that measured during the current step alone (calculated from 2 s segments of discharge before and after adding the noise stimulus; cf. Poliakov *et al.* 1996). When the discharge rate in response to the current step alone was well above the minimum firing rate, the addition of the noise stimulus produced a relatively modest increase in rate, generally less than 10%. In contrast, when the amplitude of the current step was near the threshold for repetitive discharge so that the discharge in the absence of noise was irregular, the addition of noise caused a more marked increase in the mean discharge rate. This was the case at the lowest discharge rate for the cell illustrated in Fig. 7C, and is consistent with the greater non-linear component of the transform. This finding may have important implications for the input–output properties of human motoneurones firing at low rates (see Discussion).
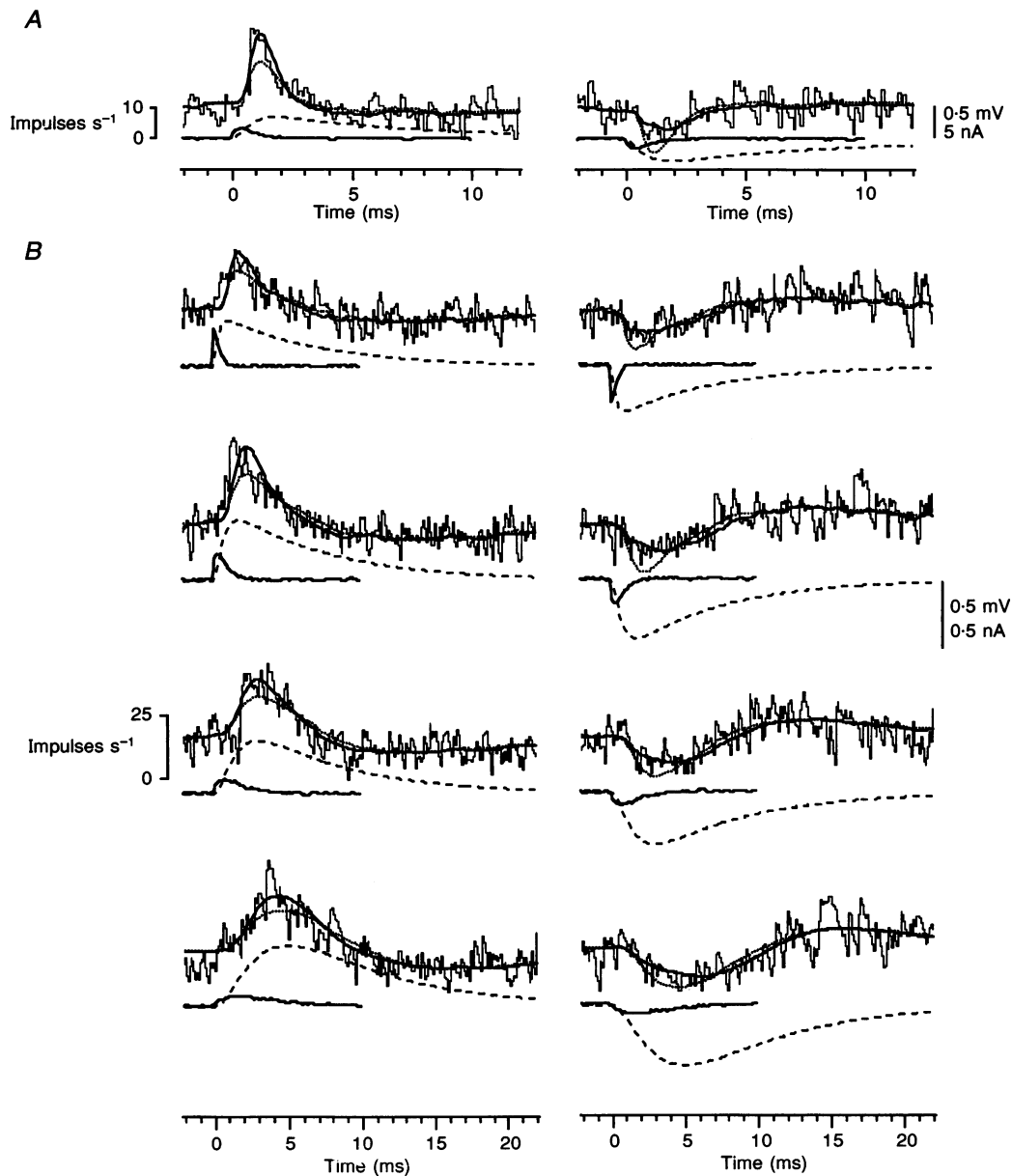
PSTHs predicted by the Wiener models

The Wiener models described above can be used to predict the motoneurone response to any arbitrary input contained within a white noise waveform (eqns (5a), (5b) and (5c)). Figure 8A illustrates the PSTHs obtained for a cat motoneurone in response to a depolarizing and a symmetric hyperpolarizing current transient (CT). As in Figs 2 and 3, the current transient waveforms are presented as the continuous traces below the PSTHs and the resultant PSPs as dashed lines. The dotted lines superimposed upon the PSTHs represent the best first-order approximations (i.e. the sum of zero- and first-order Wiener functionals; eqn (5)) of the response to the input CTs. The best second-order approximations (i.e. the sum of the zero-, first- and second-order Wiener functionals) are represented by the superimposed continuous lines. The responses to symmetric CTs predicted with the first-order model were symmetric and provided a poor match to the real PSTHs. In this and other cases, we found that the first-order model underestimated the amplitude of the response to an excitatory CT. For an inhibitory CT, the first-order model also underestimated the minimal values of PSTH troughs, often predicting negative values, which the real PSTHs could not reach. The predictions that included the second-order Wiener functional were asymmetric and provided a better match to the PSTHs for both excitatory and inhibitory CTs. Figure 8B shows the PSTHs obtained in a

rat along with the first-order (dashed lines) and second-order (continuous lines) predictions for four different excitatory CTs of various amplitudes and durations (Fig. 8B, left column), and symmetric inhibitory CTs (right column). The second-order predictions provided a good match to all of the illustrated PSTHs, whereas the first-order fits tended to underestimate the PSTH peaks produced by depolarizing

inputs and overestimate the amplitudes of the PSTH troughs produced by hyperpolarizing inputs.

The accuracy of the first-order Wiener model depended both on the background firing rate of the motoneurone and on the size of the current transient. We quantified the goodness of fit of the first- and second-order models by calculating the mean squared error (MSE) between the

Figure 8. The PSTH profiles predicted by first- and second-order Wiener models

A, the PSTHs show the responses of a cat lumbar motoneurone to a depolarizing (left) and symmetric hyperpolarizing (right) current transient. The superimposed dotted lines show the predicted PSTH based on the first-order Wiener model (i.e. the sum of the zero- and first-order Wiener functionals). The predicted PSTHs are symmetrical and feature a 'negative firing rate' in response to the inhibitory transient. The predictions of a second-order model (i.e. the sum of the zero-, first- and second-order Wiener functionals) are shown by continuous lines and provide a better match to the actual PSTHs. *B*, analogous results for a rat hypoglossal motoneurone. The underlying excitatory (left column) and inhibitory (right column) current transients had times to peak of 0·2, 0·4, 0·8 and 1·6 ms, from top to bottom. The calculated PSPs are superimposed on the current transients as dashed lines.

PSTH values predicted by the models and actual PSTHs (determined by the mean squared difference between the predicted and actual values, expressed as a percentage of the actual value, see formulas 14–16 in Sakai, 1992). To minimize the contribution of random bin fluctuations both the actual and predicted PSTHs were smoothed with a binomial filter with a time window of 1 ms, and the MSE was calculated for lags of 0–15 ms. In each case, the MSE values for the first- and second-order model predictions were compared for the PSTHs compiled for each current transient. In four of seven rat motoneurones, the MSE values for the second-order model were significantly lower than those for the first-order model (paired t value < 0·05). The most prominent differences in the accuracy of the two predictions occurred for the largest current transients. For example, the MSE values averaged across the largest ten current transients for all seven rat motoneurones were 4·4% for the first-order model and 3·4% for the second-order model, whereas the relative accuracies of the two models were identical for the PSTHs compiled from the ten smallest

current transients (3·4%). Similar comparisons were made for the three cat motoneurones, at two different background firing rates for each. The MSE for the second-order prediction was significantly lower than that of the first-order model in only one of six cases and in one case it was significantly higher due to the fact that the second-order model overestimated the PSTH peak for the larger depolarizing current transients.

The relatively small differences between the MSE values obtained for the two different models may reflect the fact that the predicted PSTHs are quite similar over much of their time course, with the most prominent differences occurring over a fairly narrow region of the PSTH peak (or trough, see Fig. 8). An alternative test of the relative accuracy of the first- and second-order Wiener models is to compare a number of features of the real PSTHs with those predicted by the models. Figure 9 compares measurements made from the actual PSTHs (x-axes) with those derived from the PSTHs predicted by three different models (y-axes)
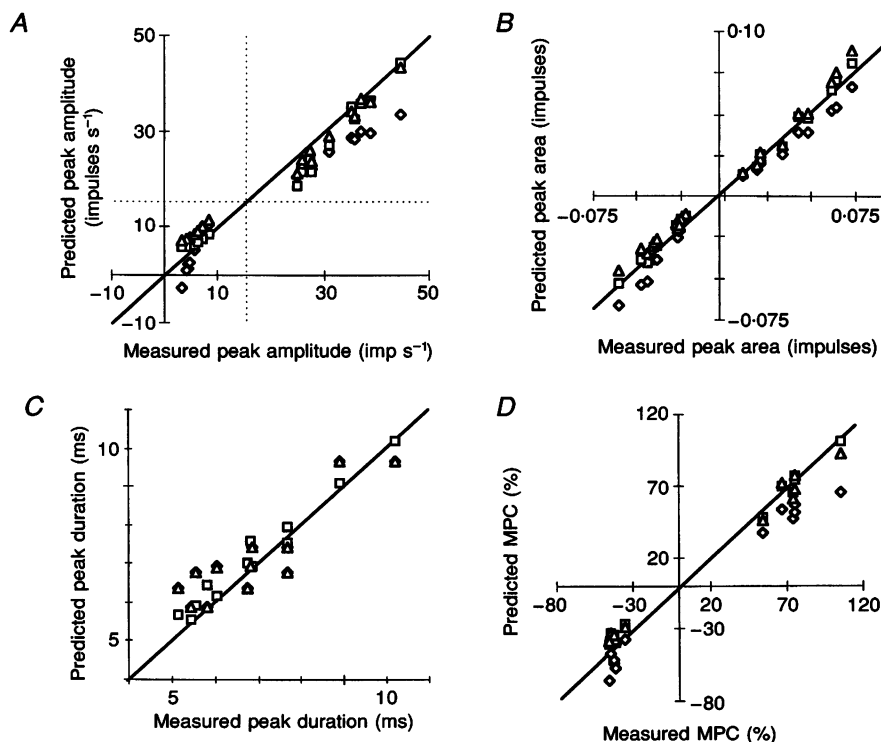

Figure 9. Comparison between the PSTHs compiled for individual current transients and those predicted by several different models

Measurement of peak amplitude (*A*), peak area (*B*), latency to peak value (*C*), and mean percentage change (MPC) in firing rate (*D*) were taken from the average PSTHs for 7 rat hypoglossal motoneurones. Each point on the graphs corresponds to a particular current transient: the abscissa is the actual average value for the corresponding PSTHs, and the ordinate is the predicted value based on the first-order Wiener model (◇), the second-order Wiener model (□), or the cascade approximation model (△). *A*, peak amplitude of the PSTHs. The intersection of the two dotted lines represents the mean background firing rate for these 7 rat motoneurones. The symbols in the upper right quadrant represent peak firing rate in response to depolarizing current transients whereas those in the lower left quadrant represent minimal firing rate in response to hyperpolarizing current transients. *B*, peak area of the PSTHs. *C*, duration of the peak/trough in the PSTHs. Only the data for the 12 largest current transients were included. *D*, mean percentage change in firing rate.

averaged across our sample of seven rat motoneurones. (As in the analysis above, both predicted and actual PSTHs were smoothed with a 1 ms filter.) In addition to the first- and second-order Wiener models, we also calculated the predicted PSTH based on the 'cascade approximation' of the second-order Wiener model (eqns (11*a*) and (11*b*)). The predictions of the three models are indicated by different symbols (first-order, ◇; second-order, □; cascade approximation, △). The thick line in each part of the figure

represents the line of identity. All three of the models provided reasonable matches to the duration of the PSTH peak (or trough; Fig. 9*C*). However, the first-order model underestimated the peak amplitude (Fig. 9*A*) of the PSTHs for large depolarizing CTs and overestimated the peak decrease in firing rate associated with hyperpolarizing CTs, predicting negative firing rates for the largest ones. Similarly, the first-order model underestimated the values of mean percentage change in firing rate (MPC; Fig. 9*D*) for
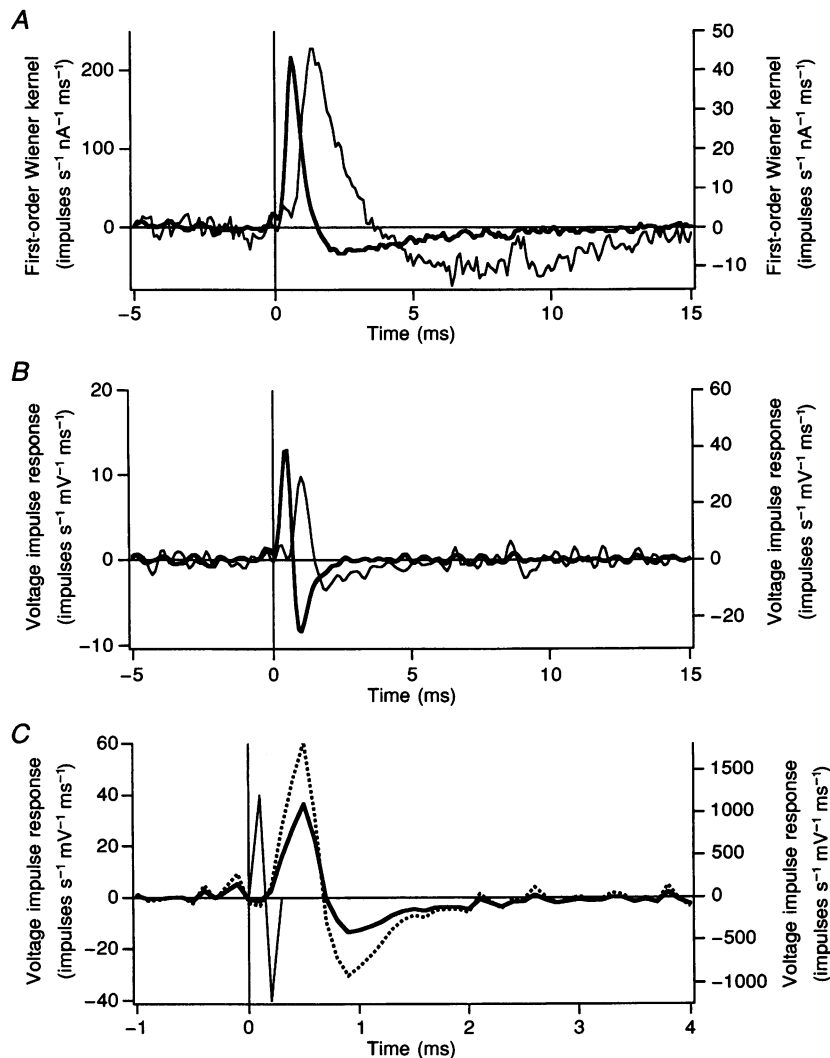
Figure 10. Impulse responses of rat hypoglossal and cat lumbar motoneurones to brief current pulses

A, first-order Wiener kernels for a cat (thick traces, right-hand axis) and a rat (thin traces, left-hand axis) motoneurone. *B*, the transform of membrane potential into firing rate. This transform was calculated by first estimating the passive membrane response of each motoneurone to a brief pulse of current and then deconvolving the passive impulse response with the first-order Wiener kernels in *A*. The deconvolution was performed by first dividing the fast Fourier transforms (FFTs) of the impulse responses by those of the passive membrane responses, and then taking the inverse FFT of the result. The plots in *B* were digitally smoothed with a three-point binomial filter included in the Igor Pro software package. *C*, comparison of cat motoneurone voltage impulse response (thick continuous line, left axis) with that of a static linear model (thin continuous line, right axis). The dotted line shows the cat motoneurone voltage impulse response obtained with a different estimate of the passive membrane response. See text for further details.

PSTHs produced with large depolarizing and hyperpolarizing CTs. For PSTH peak area (Fig. 9*B*), the errors were smaller, but showed the same trend. The second-order and the cascade models provided better matches to each parameter of PSTHs.

To evaluate the goodness-of-fit of the three models, we calculated the differences between the measured value of a particular PSTH feature and that predicted by the models for each current transient. We then computed the root mean square of these differences. (For the peak width parameter, we only included values for the twelve largest CTs, because the peak width could not be measured with confidence for some of the smallest CTs.) For the first-order, second-order and cascade models, the root mean squares of the differences between actual and predicted values were, respectively: 3·48, 2·31 and 2·55 impulses s^{-1} for PSTH peak amplitude; 5·80, 3·34 and 4·83 × 10^{-3} impulses for PSTH peak area; 0·67, 0·26 and 0·67 ms for PSTH peak width; 10·48, 6·20 and 8·67 % for MPC. Thus, for all four PSTH parameters, the root mean square errors were the smallest for the second-order Wiener model, indicating that it gave the best approximation of the actual PSTHs. The cascade model produced better approximations of the PSTH parameters than did the first-order Wiener model, with the exception of the width of the PSTH peak.

We also produced plots like those of Fig. 9 for individual cells, including the three cat lumbar motoneurones. These individual plots were all qualitatively similar to the average data, in that the predictions of the first-order model showed the largest deviations from the actual PSTH features for the largest CTs. The extent of this deviation was greatest in trials with low background firing rates.

Comparison of first-order Wiener model to other linear models of the motoneurone

The results present in Fig. 9 indicate that even the first-order Wiener model provides a good prediction of the PSTH features produced by a fairly wide range of current transients. Considering that a single set of model parameters is used to predict a range of responses, this represents a considerable improvement on previously proposed linear models (cf. Fig. 3). One common characteristic of previously proposed linear models is that the predicted value of motoneurone firing probability at a given time following a PSP depends only on the value of the PSP (and/or its derivative) at a single point in time, i.e. they are all static models. In contrast, our first-order model based on the Wiener kernels is dynamic, i.e. the probability of spike generation at a given lag depends on the PSP values at a number of points in time. To compare the predictions of our first-order model (which are functions of injected current) with those derived from previous formulations (which are expressed in terms of membrane voltage), we must first account for the transformation of injected current into

membrane voltage. Figure 10*A* illustrates representative first-order Wiener kernels for cat (thick lines, right-hand scale) and rat motoneurones (thin lines, left-hand scale). As discussed earlier, the first-order kernel is the best-fit, linear prediction of the change in firing probability produced by a brief pulse of current with an area of 1 nA ms. The changes in membrane potential produced by this same input (i.e. the passive membrane response) can be predicted from a single time constant approximation of the passive response of the rat motoneurone, and a two-time constant approximation of the response of the cat motoneurone (see Methods). Figure 10*B* illustrates the linear prediction of the change in motoneurone firing probability in response to a voltage pulse (with an area of 1 mV ms), obtained by deconvolving the first-order kernel with the passive membrane response to the current pulse (see figure legend for details). Although the duration of this voltage 'impulse response' is much briefer than the corresponding response to a current pulse (Fig. 10*A*), it still has an appreciable duration, indicating that the firing probability at a given time lag depends upon the values of membrane potential at a number of points in time, rather than on a single value of membrane potential (or its derivative). This point is made more clearly in Fig. 10*C*, which compares the cat voltage impulse response (thick continuous line, left axis) to a two-point impulse response derived from the static linear model described in eqn (6) (thin continuous line, right axis).

The differences in the cat and rat voltage impulse responses illustrated in Fig. 10*B* indicate that the different time courses of the first-order Wiener kernels between rat and cat motoneurones cannot be simply ascribed to the differences in their passive membrane properties. Although the magnitude of the voltage impulse response depends on our estimates of passive membrane properties, the time course is relatively insensitive to these estimates. This point is illustrated by comparing the voltage impulse responses for a cat motoneurone obtained when the passive membrane response was estimated from a single time constant (Fig. 10*C*, dotted line) rather than a two time constant approximation (thick continuous line). Similarly, the dependence of the kernel's time course on background firing rate (cf. Fig. 7*C* and *D*) cannot be a factor here since the Wiener kernels in Fig. 10*A* were calculated at similar background firing rates. The differences in the voltage impulse responses of Fig. 10*B* are in fact representative of the entire sample of cat and rat motoneurones. In both types of cell the voltage impulse response consisted of an initial peak followed by a smaller undershoot. However, the responses in cat motoneurones had times to peak of < 1 ms, whereas those of the rat motoneurones were 1·5–2 ms. These results indicate that there are differences in the spike encoding processes of rat hypoglossal and cat lumbar motoneurones.

DISCUSSION

We undertook this study with the intent of developing a general description of the relation between the characteristics of a transient synaptic input and its effects on the firing probability of a tonically discharging motoneurone. We used trains of injected current transients to mimic the synaptic currents produced by small numbers of repetitively discharging excitatory and inhibitory presynaptic fibres. We simulated the physiological synaptic activation of motoneurones by thousands of presynaptic inputs by embedding these trains of current transients in a suprathreshold injected current step with superimposed random noise. This synthesized current waveform served two purposes: it allowed us to compile PSTHs between the occurrences of a particular current transient and the motoneurone spike, and it provided an appropriate input signal for the calculation of zero-, first- and second-order Wiener kernels. We then tested the accuracy of several system descriptions derived from these Wiener kernels in predicting the actual PSTHs. A first-order system based on the zero- and first-order Wiener kernels provided a reasonable fit to PSTHs evoked by the smaller inputs (corresponding to single fibre PSPs), but the addition of a second-order functional was required to fit the PSTHs associated with the larger inputs.

Our results represent an extension of previous analyses of the relation between synaptic inputs and their effects on motoneurone firing probability. Based on comparisons of EPSP and PSTH shape, other investigators have proposed that the PSTH profile can be approximated by either a scaled version of PSP waveform (Moore et al. 1970), a scaled version of the PSP derivative (Knox, 1974; Fetz & Gustafsson, 1983) or a linear combination of the PSP and its derivative (Kirkwood & Sears, 1978; Gustafsson & McCrea, 1984). The empirical support for these models was based on analyses of the effects of one, or at most a few, different synaptic inputs in a given cell. Consequently, systematic comparisons of PSP and PSTH shapes required pooling data derived from many different cells. The present approach permitted us to study the effects of many differently sized and shaped PSPs recorded in the same cell under identical experimental conditions. This concurrence eliminates any possible variation in results due to differences in the intrinsic properties of the motoneurone, its background discharge rate, or the level of superimposed synaptic noise.

In agreement with previous findings (Fetz & Gustafsson, 1983; Gustafsson & McCrea, 1984; Cope et al. 1987), we found that for depolarizing inputs the PSTH peaks were generally wider than the positive phase of the PSTH derivative, but narrower than the time course of the PSP itself. As also reported by others (Gustafsson & McCrea, 1984; Cope et al. 1987), we found that the PSTHs can often be reasonably well approximated by a combination of the PSP and its derivative. However, the values of the scaling coefficients for the two terms vary widely for different inputs to the same cell. Since this variation in scaling

coefficients occurred for different inputs studied concurrently, it cannot be attributed to variations in motoneurone discharge rate or in the characteristics of the superimposed noise. Instead, our findings indicate that none of the previously proposed linear models provide a good general description of the relation between the time course of a synaptic input and its effects on discharge probability.

The impulse response of the motoneurone

The first-order Wiener model differs from previously proposed linear models of the motoneurone in that it represents spike encoding as a dynamic process, i.e. one that depends on prior values of membrane voltage. The voltage impulse responses of Fig. 10*B* provide an estimate of the relationship between membrane potential and the probability of spike generation. In a simple threshold-crossing neurone model, in which spikes are triggered whenever the membrane potential (V_m) crosses a specified threshold value (Θ), the relationship between membrane potential and the probability of a spike occurring (P_s) is a step function, i.e. $P_s = 0$ for $V_m < \Theta$ and $P_s = 1$ for $V_m \geq \Theta$. In real neurones, P_s is likely to be a sigmoidal function of V_m, reflecting the voltage dependence of sodium channel activation. Moreover, the time taken to initiate a spike will depend upon V_m. This utilization time will be longer for 'just threshold' depolarizations than for larger depolarizations (Hodgkin & Huxley, 1952). As a consequence of these two factors, the voltage impulse response of a real neurone has an appreciable duration, whereas that of a threshold-crossing model approximates a delta function. Thus, the different time courses of the voltage impulse responses in cat and rat motoneurones probably reflect differences in either the properties or spatial distribution of their voltage-gated sodium channels.

Comparisons of the time courses of the PSTHs, first-order Wiener kernels and voltage impulse responses for rat and cat motoneurones are all confounded by multiple variables. In addition to the obvious differences in animal and motoneurone species, the rat experiments were carried out using an *in vitro* preparation at room temperature, whereas the cat data were obtained *in situ* at normal body temperature. In some preliminary experiments, we altered the temperature of the bathing solution in our *in vitro* preparation by 5 °C, and found only small changes in the time course of the kernels in rat hypoglossal motoneurones (Poliakov et al. 1996). We also recorded the responses of several spinal motoneurones in the intact, adult rat and found that the time courses of the first-order kernels were virtually identical to those of the adult cat cells reported here (R. K. Powers, J. Celichowski & M. D. Binder, unpublished observations). Thus, the longer duration of the first-order kernels and voltage impulse responses in rat hypoglossal motoneurones probably reflects differences in either the intrinsic properties of this type of motoneurone or differences in the expression of cellular properties in the *in vitro* preparation.

Non-linearity in the input–output transform

The non-linear (sigmoidal) voltage dependence of sodium channel activation (Hodgkin & Huxley, 1952) may also underlie the presence of a significant non-linear component in the overall transformation of injected current to firing

probability. As noted by others (e.g. French & Korenberg, 1989), the fact that sodium channels are activated only by depolarizing inputs should lead to half-wave rectification of the output. However, in our experiments the steady depolarization produced by the suprathreshold current step probably ensured that both the hyperpolarizing and depolarizing components of the white noise signal could affect the activation of sodium channels. Nonetheless, since most of the motoneurones fired at rates close to their minimum steady discharge rate, it is likely that membrane potentials traversed during the interspike interval covered the lower range of the sodium activation curve, over which its slope increases with increasing depolarization. As a consequence, depolarizing inputs should have a more pronounced effect on spike probability than hyperpolarizing inputs, as was observed (Fig. 2). Regardless of the underlying mechanism, the short-latency peak along the main diagonal of the second-order Wiener kernel (Figs 5 and 6, parts *B* and *C*) ensures that the firing probability in response to depolarizing inputs will increase in a greater than linear fashion with increasing input magnitude, whereas the firing probability will decrease in response to hyperpolarizing inputs in a less than linear fashion with increasing input magnitude.

The other significant feature of the second-order Wiener kernels in both rat and cat motoneurones is a set of symmetrical troughs off the main diagonal. As mentioned in Results, this feature represents a non-linear interaction between the effects of two inputs occurring at different time lags. Specifically, the trough indicates that the effect of a given depolarizing input will be depressed if it is preceded at the appropriate time lag by another depolarizing input. To the extent that our approximation of the second-order kernel is valid, the efficacy of a depolarizing pulse will also be enhanced if preceded by a hyperpolarizing input (cf. eqn (10)). One possible mechanism underlying this behaviour is variation in the level of sodium channel inactivation. The voltage threshold for spike initiation in motoneurones varies during the course of the interspike interval, and the time course of this variation has a small lag with respect to membrane potential (Calvin, 1974; Powers & Binder, 1996). The time course of this variation in threshold is consistent with changes in sodium channel availability due to the voltage dependence and kinetics of initial segment sodium channel inactivation (see Powers (1993) for a detailed discussion). According to this hypothesis, a subthreshold depolarizing input would increase sodium channel inactivation for a short time following the depolarization, reducing the spike-triggering efficacy of any subsequent depolarizing input.

Comparisons with other white noise analyses of neurone input–output functions

The characteristics of the Wiener kernels calculated from our data differ somewhat from those reported previously for cat spinal motoneurones (Boskov, Jocic, Jovanovic, Ljubisavljevic & Anastasijevic, 1994) and catfish retinal

ganglion cells (Korenberg, Sakai & Naka, 1989). In both of these studies, the authors concluded that the dynamics of spike encoding contributed little to the transformation of synaptic potentials to changes in firing probability. However, these studies were concerned with spike encoding where the dynamics of the input–output transformation are largely due to the properties of neural elements that are presynaptic to the spike-generating neurone (either a change in muscle length or applied light intensity).

In the experiments performed by Boskov *et al.* (1994), the white noise injected currents were generally larger than those used here, and no depolarizing bias current was added. Both bias current and noise amplitude have been shown to affect the shape of the average spike-evoking current waveform (Bryant & Segundo, 1976) and thus, these factors may be responsible for the differences between the shapes of our first-order kernels and those reported by Boskov *et al.* (1994). In addition, both the form and the magnitude of the second-order kernel may also differ since, as noted above, in the absence of a depolarizing bias the hyperpolarizing component of the white noise stimulus will have little or no effect on the probability of spike generation.

Our method of testing the accuracy of our Wiener model approximations also differs from that of several previous studies. The white noise method of system identification has been most commonly applied to systems in which both the input and output are continuous variables (Marmarelis & Marmarelis, 1978; Sakai, 1992, for review). In the case of a discontinuous output (i.e. a series of spikes), one can test the accuracy of the Wiener approximation by converting the predicted output to a series of spikes by assuming that a spike will occur whenever the output exceeds a fixed threshold (e.g. Korenberg, French & Voo, 1988). The alternative method used here, which was originally devised by Moore & Auriemma (1985), was to obtain a continuous output by compiling PSTHs in response to the repetitive application of a transient waveform embedded in the background noise. The novel feature introduced in our experiments was to embed a variety of current transient waveforms within our noise stimulus, allowing us to test the accuracy of the first- and second-order Wiener model as a function of the time course and magnitude of the current transients.

The reasonably good fits that we found between the first-order Wiener prediction and the PSTHs evoked by small current transients indicates that a linear model of spike encoding provides a good approximation to the responses evoked in motoneurones by one or a few presynaptic fibres. The inaccuracies of the previously proposed linear models probably reflects the fact that they are all static (zero-memory) transforms. For the larger current transients, we found that there was a significant improvement in accuracy of the predicted responses when a non-linear, second-order functional was added to the model.

Summary, applications and limitations

The results of our study strongly suggest that compiling PSTHs between one or even a few identified synaptic inputs and the discharge of a postsynaptic neurone does not provide enough information to identify the general input–output function of the neurone. We have shown, however, that the white noise method of systems identification can be used quite effectively to yield both the best linear approximation of the input–output function of a neurone, as well as a more complete, higher-order description of its spike-encoding behaviour. We found that truncating the Wiener series at the second-order functional was sufficient to capture both the linear and principal non-linear components of the input–output transform. Further, the contribution of the second-order Wiener functional could be approximated simply by substituting a parabolic transform of the convolution integral of the input signal with the first-order kernel (eqn (11)) for the second-order Wiener functional. This Wiener cascade model accurately predicted the responses of motoneurones to a wide range of synaptic inputs and provided a substantial improvement over the best-fit linear model. Thus, by simply calculating the mean firing rate of the motoneurone during the application of a white noise input (i.e. the zero-order kernel) and compiling a cross-correlation of the output spike train with the white noise input signal, one can derive a general expression for the input–output function the cell.

Our enthusiasm for the white noise analysis is tempered somewhat by three limitations. First, the features of the Wiener kernels are likely to be dependent on the power of the white noise stimulus. The power levels we chose were designed to produce interspike interval distributions similar to those observed in human motoneurones during voluntary activation (i.e. coefficients of variation of the order of 10–20%; e.g. Person & Kudina, 1972). This suggests that our Wiener kernel descriptions are likely to be appropriate under most conditions of synaptic activation of moto-neurones, but may not be accurate when the variability of the synaptic noise is particularly high or low. Second, the relative contribution of the non-linear term to the input–output transform is constant over a wide range of background discharge rates, but appears to be greater when the level of the background current step is insufficient to produce regular, repetitive discharge. This situation may be analogous to the lower range of discharge rates reported in voluntarily activated human motoneurones, where many of the interspike intervals may be significantly longer than the post-spike after-hyperpolarization of the motoneurone (Matthews, 1996). Finally, the second-order model often overestimates the increase in firing probability produced by the largest depolarizing current transients, suggesting that as the amplitude of the input increases, third- and higher-order non-linearities may be important. Nonetheless, the representation of the transduction of synaptic inputs into changes in neural discharge rate as a Wiener system represents a substantial advance over previous empirical formulations. Moreover, the functional identification of neuronal input–output functions using a Gaussian white noise input signal is quite economical both in terms of the requisite data and subsequent computation time.

APPENDIX

The white noise method of system identification requires an input waveform that approximates bandwidth-limited white noise (Marmarelis & Marmarelis, 1978). The CT waveform that we formed by adding together Poisson trains of twenty different current transients is clearly a random process, but does not meet the criteria of white noise, i.e. a Gaussian distribution of amplitudes and a flat power spectrum (cf. Fig. 1C and D, thick lines). Thus, we synthesized a white noise (WN) waveform from the CT waveform by adding to it an independent random process, $y(t)$:

$$WN = CT + y(t) \qquad (A1)$$

The power spectral density of $y(t)$ compensated for the fall-off in power of the CT waveform at higher frequencies (Fig. 1D).

The initial step in this process was to generate a waveform, $x(t)$, with the properties of white noise using the following recurrent formula:

$$x_{i+1} = (1/2)x_i + \sigma(3/4)^{\frac{1}{2}} \text{Rand}(1) \qquad (A2)$$

where Rand(1) is a Gaussian random number with variance 1. The waveform $x(t)$ is a good approximation of bandwidth-limited white noise with a standard deviation of σ. Note that this random process is different from a commonly used Constant Switching Pace Random Signal (Marmarelis & Marmarelis, 1978), for which every value is an independent Gaussian random number. The autocorrelation function (a_i) of the waveform $x(t)$ is:

$$a_i = \sigma 2^{-|i|}. \qquad (A3)$$

The power (P) of $x(t)$ is:

$$P_{x(t)} = \Delta \sum_{-\infty}^{+\infty} a_i = \Delta \sigma^2 \left(1 + 2\left(\frac{1}{2} + \frac{1}{4} + \frac{1}{8} + ...\right)\right) = 3\Delta\sigma^2, \quad (A4)$$

where $\Delta = 0.1$ ms, the sampling interval.

To produce the WN waveform that included the CT waveform and had the same characteristics as the waveform $x(t)$, we had to create the waveform $y(t)$. The frequency spectrum $X(f)$ of the waveform $x(t)$ was found using the fast Fourier transform. The waveform $x(t)$, as well as waveforms CT and WN, had 2^{18} samples (26·2144 s at 10 kHz sampling rate). The frequency variable f would therefore cover the range 0–5000 Hz with $2^{17} + 1$ samples. We then calculated the power density spectrum of the CT waveform, $P_{CT}(\Phi)$, and that of the $x(t)$ waveform, $P_{x(t)}(\Phi)$. But, for these calculations, we used a lower resolution: variable Φ covers the same frequency range as f (0–5000 Hz), but with only $2^7 + 1 = 129$ samples. By choosing the standard deviation value $\sigma = 2.5$ nA,

$P_{CT}(\Phi) < P_{x(t)}(\Phi)$ for all values of Φ. We then calculated the frequency spectrum of $Y(f)$ from that of $X(f)$ using the formula:

$$Y(f) = X(f)(1 - P_{CT}(\Phi)/P_{x(t)}(\Phi)), \quad \Phi \text{ nearest to } f. \quad (A5)$$

This procedure ensured that $P_y(\Phi)$, the power density of the spectrum $Y(f)$, is:

$$P_y(\Phi) = P_{x(t)}(\Phi)(1 - P_{CT}(\Phi)/P_{x(t)}(\Phi))$$
$$= P_{x(t)}(\Phi) - P_{CT}(\Phi) \quad (A6)$$

The independent random process $y(t)$ could then be generated by applying the inverse fast Fourier transform to $Y(f)$. Its spectrum was calculated by scaling the spectrum of $X(f)$ with the coefficient $1 - P_{CT}(\Phi)/P_{x(t)}(\Phi)$. Since the power spectrum $P_{CT}(\Phi)$ has only 129 samples, it contains very little of the CT waveform. The WN waveform was then formed by adding $y(t)$ to the CT waveform, as shown by eqn (A1). $P_{WN}(\Phi)$, the power density spectrum of WN waveform is:

$$P_{WN}(\Phi) = P_{ct}(\Phi) + P_{y(t)}(\Phi)$$
$$= P_{ct}(\Phi) + (P_{x(t)}(\Phi) - P_{ct}(\Phi))$$
$$= P_{x(t)}(\Phi). \quad (A7)$$

Thus, the WN waveform has the power density of the waveform $x(t)$, which was generated to meet the criteria for bandwidth-limited white noise. The autocorrelation function and amplitude probability density of the two waveforms were also nearly equivalent.

BINDER, M. D., HECKMAN, C. J. & POWERS, R. K. (1996). The physiological control of motoneuron activity. In *Handbook of Physiology*, section 12, *Exercise: Regulation and Integration of Multiple Systems*, ed. ROWELL, L. B. & SHEPHERD, J. T., pp. 3–53. Oxford University Press, New York.

BOSKOV, D., JOCIC, M., JOVANOVIC, K., LJUBISAVLJEVIC, M. & ANASTASIJEVIC, R. (1994). Spike discharges of skeletomotor neurons during random noise modulated transmembrane current stimulation and muscle stretch. *Biological Cybernetics* **71**, 341–348.

BRYANT, H. L. & SEGUNDO, J. P. (1976). Spike initiation by transmembrane current: a white noise analysis. *Journal of Physiology* **260**, 279–314.

CALVIN, W. H. (1974). Three modes of repetitive firing and the role of threshold time course between spikes. *Brain Research* **69**, 341–346.

CONWAY, B. A., HALLIDAY, D. M. & ROSENBERG, J. R. (1993). Detection of weak synaptic interactions between single Ia afferent and motor-unit spike trains in the decerebrate cat. *Journal of Physiology* **471**, 379–409.

COPE, T. C., FETZ, E. E. & MATSUMURA, M. (1987). Cross-correlation assessment of synaptic strength of single Ia fibre connections with triceps surae motoneurones in cats. *Journal of Physiology* **390**, 161–188.

ELLAWAY, P. H. (1978). Cumulative sum technique and its application to the analysis of peristimulus time histograms. *Electroencephalography and Clinical Neurophysiology* **45**, 302–304.

FETZ, E. E., CHENEY, P. D., MEWES, K. & PALMER, S. (1989). Control of forelimb muscle activity by populations of corticomotoneuronal and rubromotoneuronal cells. *Progress in Brain Research* **80**, 437–449.

FETZ, E. E. & GUSTAFSSON, B. (1983). Relation between shapes of post-synaptic potentials and changes in firing probability of cat motoneurones. *Journal of Physiology* **341**, 387–410.

FRENCH, A. S. & KORENBERG, M. J. (1989). A nonlinear cascade model for action potential encoding in an insect sensory neuron. *Biophysical Journal* **55**, 655–661.

GUSTAFSSON, B. & McCREA, D. (1984). Influence of stretch-evoked synaptic potentials on firing probability of cat spinal motoneurones. *Journal of Physiology* **347**, 431–451.

HADDAD, G. G., DONNELLY, D. F. & GETTING, P. A. (1990). Biophysical properties of hypoglossal neurons *in vitro*: intracellular studies in adult and neonatal rats. *Journal of Applied Physiology* **69**, 1509–1517.

HODGKIN, A. L. & HUXLEY, A. F. (1952). A quantitative description of membrane current and its application to conduction and excitation in nerve. *Journal of Physiology* **116**, 500–544.

HUNTER, I. W. & KORENBERG, M. J. (1986). The identification of nonlinear biological systems: Wiener and Hammerstein cascade models. *Biological Cybernetics* **55**, 135–144.

KIRKWOOD, P. A. (1979). On the use and interpretation of cross-correlation measurements in the mammalian central nervous system. *Journal of Neuroscience Methods* **1**, 107–132.

KIRKWOOD, P. A. & SEARS, T. A. (1978). The synaptic connexions to intercostal motoneurones as revealed by the average common excitation potential. *Journal of Physiology* **275**, 103–134.

KNOX, C. K. (1974). Cross-correlation functions for a neuronal model. *Biophysical Journal* **14**, 567–582.

KNOX, C. K. & POPPELE, R. E. (1977). Correlation analysis of stimulus-evoked changes in excitability of spontaneously firing neurons. *Journal of Neurophysiology* **40**, 616–625.

KORENBERG, M. J., FRENCH, A. S. & VOO, S. K. (1988). White-noise analysis of nonlinear behavior in an insect sensory neuron: kernel and cascade approaches. *Biological Cybernetics* **58**, 313–320.

KORENBERG, M. J., SAKAI, H. M. & NAKA, K. (1989). Dissection of the neuron network in the catfish inner retina. III. Interpretation of spike kernels. *Journal of Neurophysiology* **61**, 1110–1120.

LEE, Y. W. & SCHETZEN, M. (1965). Measurement of the Wiener kernels of a non-linear system by cross-correlation. *International Journal of Control* **2**, 237–254.

MARMARELIS, P. Z. & MARMARELIS, V. Z. (1978). *Analysis of Physiological Systems: The White Noise Approach*. Plenum Press, New York.

MATTHEWS, P. B. C. (1996). Relationship of firing intervals of human motor units to the trajectory of post-spike after-hyperpolarization and synaptic noise. *Journal of Physiology* **492**, 597–628.

MOORE, G. P. & AURIEMMA, R. A. (1985). Prediction of muscle stretch receptor behavior using Wiener kernels. *Brain Research* **331**, 185–189.

MOORE, G. P., PERKEL, D. H. & SEGUNDO, J. P. (1966). Statistical analysis and functional interpretation of neuronal spike data. *Annual Review of Physiology* **28**, 493–522.

MOORE, G. P., SEGUNDO, J. P., PERKEL, D. H. & LEVITAN, H. (1970). Statistical signs of synaptic interaction in neurons. *Biophysical Journal* **10**, 876–900.

PERSON, R. S. & KUDINA, L. P. (1972). Discharge frequency and discharge pattern of human motor units during voluntary contraction of muscle. *Electroencephalography and Clinical Neurophysiology* **32**, 471–483.

POLIAKOV, A. V., POWERS, R. K. & BINDER, M. D. (1996). Dynamic responses of motoneurons to current transients studied with the white noise method. *Society for Neuroscience Abstracts* **22**, 1845.

POLIAKOV, A. V., POWERS, R. K., SAWCZUK, A. & BINDER, M. D. (1995). Effects of simulated synaptic noise on cross-correlogram features in motoneurons. *Society for Neuroscience Abstracts* **21**, 144.

POLIAKOV, A. V., POWERS, R. K., SAWCZUK, A. & BINDER, M. D. (1996). Effects of background noise on the response of rat and cat motoneurones to excitatory current transients. *Journal of Physiology* **495**, 143–157.

POWERS, R. K. (1993). A variable-threshold motoneurone model that incorporates time- and voltage-dependent potassium and calcium conductances. *Journal of Neurophysiology* **70**, 246–262.

POWERS, R. K. & BINDER, M. D. (1996). Experimental evaluation of input-output models of motoneurone discharge. *Journal of Neurophysiology* **75**, 367–379.

RALL, W. (1967). Distinguishing theoretical synaptic potentials computed for different soma-dendritic distribution of synaptic input. *Journal of Neurophysiology* **30**, 1138–1168.

RALL, W. (1969). Time constants and electrotonic length of membrane cylinders and neurons. *Biophysical Journal* **9**, 1483–1508.

REYES, A. D. & FETZ, E. E. (1993). Effects of transient depolarizing potentials on the firing rate of cat neocortical neurons. *Journal of Neurophysiology* **69**, 1673–1683.

SAKAI, H. M. (1992). White-noise analysis in neurophysiology. *Physiological Reviews* **72**, 491–505.

SAWCZUK, A., POWERS, R. K. & BINDER, M. D. (1995). Spike frequency adaptation studied in hypoglossal motoneurones of the rat. *Journal of Neurophysiology* **73**, 1799–1810.

STUART, G. J. & REDMAN, S. J. (1990). Voltage dependence of Ia inhibitory currents in cat spinal motoneurones. *Journal of Physiology* **420**, 111–125.

VIANA, F., BAYLISS, D. A. & BERGER, A. J. (1994). Postnatal changes in rat hypoglossal motoneurone membrane properties. *Neuroscience* **59**, 131–148.

VIANA, F., BAYLISS, D. A. & BERGER, A. J. (1995). Repetitive firing properties of developing rat brainstem motoneurones. *Journal of Physiology* **486**, 745–761.

Author's present address

A. Poliakov: Department of Neurology, University of Rochester, Rochester, NY 14642, USA.

Author's email address

M. D. Binder: mdbinder@u.washington.edu